UNIVERSIDADE
BEIRA INTERIOR

Development of graphene oxide-based hydrogels for cancer therapy

Francisco José Palácio Costa

Dissertação para obtenção do Grau de Mestre em
Biotecnologia
(2º ciclo de estudos)

Orientador: Professor Doutor Ilídio Joaquim Sobreira Correia
Co-orientador: Doutor Duarte Miguel de Melo Diogo
Co-orientador: Mestre Ana Rita Lima Sousa

outubro de 2022

Declaração de Integridade

Eu, Francisco José Palácio Costa, que abaixo assino, estudante com o número de inscrição M10726 de Biotecnologia da Faculdade de Ciências, declaro ter desenvolvido o presente trabalho e elaborado o presente texto em total consonância com o **Código de Integridades da Universidade da Beira Interior**.

Mais concretamente afirmo não ter incorrido em qualquer das variedades de Fraude Académica, e que aqui declaro conhecer, que em particular atendi à exigida referenciação de frases, extratos, imagens e outras formas de trabalho intelectual, e assumindo assim na íntegra as responsabilidades da autoria.

Universidade da Beira Interior, Covilhã 05 / 10 / 2022

Assinado por: **FRANCISCO JOSÉ PALÁCIO COSTA**
Num. de Identificação: 14687074
Data: 2022.10.05 10:04:49+01'00'

“I have not failed. I’ve just found 10,000 ways that won’t work.”

-Thomas Edison

Aos meus pais, à minha namorada e à minha família, que sempre acreditaram em mim... e àqueles cujas memórias carrego no coração.

Acknowledgements

Em primeiro lugar, agradeço ao Professor Doutor Ilídio Correia, meu orientador, por ter aberto as portas para me integrar no seu grupo de investigação. O seu apoio, os conselhos, a exigência e o rigor sempre presentes, foram fundamentais para conseguir desenvolver este trabalho até ao fim da melhor forma possível. Agradeço por me ter dado a oportunidade de crescer tanto profissional como pessoalmente, com a sua mão aberta sempre presente e pronta a ajudar.

Ao meu co-orientador, Doutor Duarte Diogo, um simples agradecimento parece pouco. Um imenso obrigado pela paciência, esforço e dedicação que tiveste ao longo deste ano, e por acreditares em mim até ao fim. Agradeço pelos conhecimentos que me foste transmitindo, por conseguires encontrar sempre a melhor solução para as imensas pedras que foram surgindo, e por teres dado tudo de ti até ao fim, para puder tirar o melhor desta dissertação. A tua ajuda, motivação constante e ombro amigo nos piores momentos, não serão esquecidos.

À Mestre Rita Sousa, minha co-orientadora, a quem palavras não chegam para agradecer. A tua dedicação constante foi o meu maior suporte, sem a tua ajuda não teria conseguido chegar até aqui. Mil e um obrigados por me ensinares de tudo e mais alguma coisa, por teres estado comigo a ajudar-me durante horas a fio, por teres tido paciência e por estares sempre aqui comigo. Sei que foi preciso um esforço incansável durante este ano para conciliar tudo, só tenho a agradecer o sacrifício que tiveste para me apoiares desta forma incrível.

Ao restante grupo de investigação, um enorme obrigado por todo o apoio e amizade que partilharam, e pelo vosso companheirismo nos melhores e piores momentos. Um especial obrigado à Adriana, ao André e à Micaela, pelo carinho, cumplicidade, suporte incondicional e felicidade que me trouxeram, que tornaram este ano numa experiência incrível. Conheci-vos como amigos, mas levo-vos como família.

Em especial, obrigado do fundo do coração aos meus pais, os pilares da minha vida, que se sacrificam todos os dias para me apoiar, incondicionalmente, com um sorriso na cara mesmo em dias sombrios. Obrigado pelo vosso amor e dedicação, que sem eles não teria chegado até aqui. À Estefânia, a minha companheira de coração, que me tem segurado o chão nos piores momentos com o seu amor, um obrigado mais forte que as palavras, por

todo o carinho e força que tens partilhado comigo. E, por fim, quero agradecer à minha família, que me viu crescer e partilha algo do que me tornei hoje.

Àqueles que são agora memórias que guardo no coração, dedico-vos esta vitória, como agradecimento de tudo o vivemos juntos.

Resumo

A nível mundial, o cancro da mama continua a ser uma das principais causas de morte especialmente nas mulheres. A alta mortalidade desta doença está fortemente associada às limitações das terapias atualmente usadas em meio clínico, como a cirurgia, quimioterapia e radioterapia. Estas modalidades terapêuticas apresentam uma baixa eficácia e induzem diversos efeitos secundários no ser humano. Tais fatores revelam a necessidade de desenvolver novas terapias que sejam mais eficazes no tratamento desta doença.

Neste contexto, ao longo dos anos, os investigadores têm desenvolvido diversos tipos de nanomateriais (p. ex. dendrímeros, lipossomas, micelas) para aplicação em diferentes modalidades terapêuticas anticancerígenas. Recentemente, as atenções voltaram-se para os nanomateriais com capacidade fototérmica. Estes, quando interagem com a luz com um comprimento de onda no infravermelho próximo (em inglês: *Near Infrared* (NIR); 750 – 1000 nm), conseguem absorver a sua energia, libertando-a sob a forma de calor, que pode induzir dano nas células cancerígenas. Os nanomateriais responsivos à luz NIR conseguem ainda encapsular fármacos, possibilitando o seu uso em terapia combinatória. Estes são geralmente administrados por injeção intravenosa. Contudo, os nanomateriais administrados por via sistémica são incapazes de atingir o tumor em quantidades elevadas, não tendo assim o efeito o terapêutico desejado.

Desta forma, estão a ser desenvolvidas novas tecnologias capazes de entregar as nanopartículas diretamente no tecido tumoral. Em particular, os hidrogéis formados através de reações de adição tipo Michael entre os grupos Tiol e Maleimida adequam-se a esta aplicação devido à sua capacidade para incorporar altas doses de nanopartículas na sua estrutura 3D compacta. Para além disto, estes apresentam uma boa seletividade química, biocompatibilidade, e preparação simples. No entanto, os referidos hidrogéis têm sido, na sua maioria, preparados recorrendo a polímeros sintéticos, sendo que este fator não é ideal considerando a fraca biodegradabilidade destas moléculas.

No trabalho de investigação desenvolvido no 2º ano deste ciclo de estudos, foi produzido um novo hidrogel, tendo por base polímeros naturais e posterior reticulação através da ligação Tiol-Maleimida, para aplicação na terapia quimio-fototérmica de células do cancro da mama. De modo que fossem obtidos polímeros naturais compatíveis com esta química de reticulação, o Ácido Hialurónico foi funcionalizado com grupos Tiol e o Quitosano desacetilado foi imobilizado com grupos Maleimida. Simultaneamente, o

Óxido de Grafeno reduzido com Dopamina foi produzido e encapsulado com Doxorrubicina (DOX/DOPA-rGO), de forma a criar-se um nanomaterial responsivo à luz NIR com propriedades quimio-fototérmicas.

Posteriormente, os hidrogéis reticulados pela ligação Tiol-Maleimida contendo este nano-agente terapêutico (DOX/DOPA-rGO@TMgel) foram preparados através de uma mistura simples dos seus precursores (Ácido Hialurónico-Tiol, Quitosano desacetilado-Maleimida e DOX/DOPA-rGO). Nos estudos *in vitro*, os resultados obtidos demonstraram que as células do cancro da mama expostas ao DOPA-rGO@TMgel juntamente com luz NIR tiveram uma redução na sua viabilidade para cerca de 59 %. Por outro lado, o DOX/DOPA-rGO@TMgel provocou uma redução na viabilidade das células cancerígenas para 50 %. Em contraste, a ação combinada do DOX/DOPA-rGO@TMgel com a luz NIR conseguiu reduzir a viabilidade das células cancerígenas da mama para apenas 21 %, salientando o seu potencial para a terapia quimio-fototérmica.

Palavras-chave

Cancro;Hidrogéis Tiol-Maleimida;Nanomateriais da família do grafeno;Sistemas de entrega à macro-escala;Terapia quimio-fototérmica.

Resumo Alargado

O cancro continua a ser uma das doenças mais devastadoras para a saúde humana. Em especial, o cancro da mama apresenta-se como sendo bastante preocupante uma vez que, para além de ser o cancro mais incidente no sexo feminino, é também aquele que apresenta uma maior taxa de mortalidade. Esta elevada mortalidade deve-se principalmente à baixa eficácia das terapias convencionais usadas em meio clínico, como a cirurgia, quimioterapia ou radioterapia. Estas terapias trazem ainda efeitos adversos ao ser humano, associados à toxicidade sistémica das mesmas. Existe assim uma urgência no desenvolvimento de novas modalidades terapêuticas mais eficazes para combater esta doença.

Neste contexto, ao longo dos anos, os investigadores têm desenvolvido diversos tipos de nanomateriais (p. ex. dendrímeros, lipossomas, micelas) para aplicação em diferentes modalidades terapêuticas anticancerígenas. Em particular, os nanomateriais com capacidade fototérmica têm tido especial destaque. Estes conseguem, após interagir com luz com comprimento onda no infravermelho próximo (do inglês: *Near Infrared* (NIR); 750 – 1000 nm), produzir um aumento de temperatura que pode induzir dano nas células cancerígenas. As nanopartículas responsivas à luz NIR podem ainda encapsular agentes terapêuticos, como fármacos, permitindo a sua aplicação em terapia combinatória. Contudo, estes nanomateriais são geralmente administrados por injeção intravenosa. Tal facto apresenta-se como não sendo ideal, uma vez que os nanomateriais administrados sistemicamente têm-se revelado incapazes de atingir o tumor em quantidades elevadas, não atingindo assim o efeito terapêutico desejado.

Atualmente, estão a ser investigadas novas tecnologias com a capacidade de entregar as nanopartículas diretamente no tecido tumoral. Neste contexto, os hidrogéis formados através de reações de adição tipo Michael entre os grupos Tiol e Maleimida apresentam-se como promissores. Este tipo de sistema de entrega à macro-escala possui capacidade de incorporar elevadas doses de nanopartículas na sua estrutura 3D compacta. Para além disto, este tipo de hidrogel apresenta uma boa seletividade química, biocompatibilidade, e uma preparação simples sem uso de iniciadores tóxicos. No entanto, estes hidrogéis têm sido, na sua maioria, preparados recorrendo a polímeros sintéticos, cuja fraca biodegradabilidade é um fator limitante no seu uso clínico.

No trabalho de investigação desenvolvido no 2º ano deste ciclo de estudos, foi produzido um novo hidrogel, com base em polímeros naturais e posteriormente foi reticulado

através de ligações Tiol-Maleimida, para aplicação na terapia quimio-fototérmica de células do cancro da mama. De modo que fossem obtidos polímeros naturais compatíveis com esta química de reticulação, o Ácido Hialurónico foi funcionalizado com grupos Tiol e o Quitosano desacetilado foi imobilizado com grupos Maleimida. Simultaneamente, o Óxido de Grafeno reduzido com Dopamina foi produzido e encapsulado com Doxorrubicina (DOX/DOPA-rGO), de forma a criar-se um nanomaterial responsivo à luz NIR com propriedades quimio-fototérmicas.

Posteriormente, os hidrogéis reticulados pela ligação Tiol-Maleimida contendo este nano-agente terapêutico (DOX/DOPA-rGO@TMgel) foram preparados através de uma mistura simples dos seus precursores (Ácido Hialurónico-Tiol, Quitosano desacetilado-Maleimida e DOX/DOPA-rGO). Os hidrogéis apresentaram gelificação adequada e uma boa porosidade. Quando expostos à radiação NIR, estes conseguiram induzir um aumento de temperatura de cerca de 22 °C. Nos estudos *in vitro*, os resultados obtidos demonstraram que o DOPA-rGO@TMgel (hidrogel controlo sem DOX) apresenta uma boa citocompatibilidade, tanto em células saudáveis como em células do cancro da mama. Observou-se ainda que as células do cancro da mama expostas ao DOPA-rGO@TMgel juntamente com luz NIR (terapia fototérmica) tiveram a sua viabilidade reduzida para cerca de 59 %. Por outro lado, o DOX/DOPA-rGO@TMgel (quimioterapia) provocou uma redução na viabilidade das células cancerígenas para 50 %. Em contraste, a ação combinada do DOX/DOPA-rGO@TMgel com a luz NIR conseguiu reduzir a viabilidade das células cancerígenas da mama para apenas 21 %, salientando o seu potencial para a terapia quimio-fototérmica.

Abstract

Breast cancer is a major cause of death of women worldwide. This high mortality rate is a consequence of the limitations of the currently used therapies, such as surgery, chemotherapy and radiotherapy. Such therapies exhibit a poor efficacy and induce several side effects. Therefore, the development of new therapies is imperative.

Along the years, researchers have developed several types of nanomaterials (*e.g.* dendrimers, liposomes, micelles) for application in different anticancer modalities. Recently, the focus has turned towards the photothermal capacity of some nanomaterials. When irradiated with Near Infrared (NIR; 750 – 1000 nm) light, these nanomaterials can absorb its energy, releasing it as heat that induces damage in cancer cells. These light-responsive nanomaterials can also accommodate drugs in their structure, enabling their use in combinatorial therapeutic approaches. However, the nanomaterials are commonly administered by intravenous injection, which is not ideal considering the weak tumor-homing capacity of systemically administered nanomaterials, leading to a subpar outcome.

Due to that, new technologies capable of delivering nanoparticles directly into the tumor tissue are under investigation. In particular, hydrogels formed through Thiol-Maleimide Michael type additions display potential to this application owing to their ability to incorporate high doses of nanoparticles into their compact 3D structure, as well as good chemical selectivity, biocompatibility, and simple production. However, such hydrogels have been mostly prepared using synthetic polymers, which are not ideal considering their non-biodegradability.

Herein, a novel Thiol-Maleimide crosslinked hydrogel, engineered using natural polymers, was produced for application in the chemo-photothermal therapy of breast cancer cells. To obtain natural polymers compatible with this crosslinking chemistry, Hyaluronic Acid was decorated with Thiol groups and deacetylated Chitosan was grafted with Maleimide groups. Simultaneously, Dopamine-reduced Graphene Oxide was produced and loaded with Doxorubicin (DOX/DOPA-rGO) to create NIR light responsive nanomaterial with chemo-photothermal capabilities. In order to formulate the Thiol-Maleimide crosslinked hydrogels incorporating this therapeutic nano-agent (DOX/DOPA-rGO@TMgel), a simple mixture of Hyaluronic acid-Thiol, deacetylated Chitosan-Maleimide and DOX/DOPA-rGO was performed. In *in vitro* studies, when breast cancer cells were incubated with DOPA-rGO@TMgel and exposed to NIR light

(photothermal therapy), their viability was reduced to about 59 %. On the other hand, DOX/DOPA-rGO@TMgel (chemotherapy) reduced cancer cells' viability to 50 %. In stark contrast, the combined action of DOX/DOPA-rGO@TMgel and NIR light decreased breast cancer cells' viability to just 21 %, highlighting its chemo-phototherapeutic potential.

Keywords

Cancer, Chemo-photothermal therapy, Graphene family nanomaterials, Macro-scale delivery systems, Thiol-Maleimide hydrogels.

List of Publications

Articles submitted for publication in international peer reviewed journals:

Rita Lima-Sousa, Cátia G. Alves, Bruna L. Melo, Francisco J. P. Costa, Micaela Nave, André F. Moreira, António G. Mendonça, Ilídio J. Correia, Duarte de Melo-Diogo. Injectable hydrogels for the delivery of nanomaterials aimed for cancer combinatorial photothermal therapy. *Under review*.

Francisco J. P. Costa, Micaela Nave, Rita Lima-Sousa, Cátia G. Alves, Bruna L. Melo, Ilídio J. Correia, Duarte de Melo-Diogo. Development of Thiol-Maleimide hydrogels incorporating graphene-based nanomaterials for cancer chemo-photothermal therapy. *Submitted*.

Micaela Nave, Francisco J. P. Costa, Cátia G. Alves, Rita Lima-Sousa, Bruna L. Melo, Ilídio J. Correia, Duarte de Melo-Diogo. Simple preparation of POxylated nanomaterials for cancer chemo-PDT/PTT. *Submitted*.

Index

Chapter 5

Chapter 6

Figure Index

List of Abbreviations

^{1}H NMR	Proton nuclear magnetic resonance
ANOVA	Analysis of variance
Ch	Chitosan
Chemo-PTT	Chemo-Photothermal Therapy
CLSM	Confocal Laser Scanning Microscopy
dCh	Deacetylated Chitosan
dCh-Mal	Maleimide-grafted deacetylated Chitosan
DLS	Dynamic Light Scattering
DMEM-F12	Dulbecco's Modified Eagle's Medium F-12
DOPA-rGO	Dopamine-reduced Graphene Oxide
DOPA-rGO@TMgel	Thiol-Maleimide HA-Ch based hydrogel incorporating DOPA-rGO
DOX	Doxorubicin
DOX/DOPA-rGO	Doxorubicin loaded DOPA-rGO
DOX/DOPA-rGO@TMgel	Thiol-Maleimide HA-Ch based hydrogel incorporating DOX/DOPA-rGO
EDC	1-Ethyl-3-(3-dimethylaminopropyl) carbodiimide
EPR	Enhanced Permeability and Retention
FBS	Fetal Bovine Serum
FTIR	Fourier Transform Infrared
GO	Graphene Oxide
HA	Hyaluronic Acid
HA-Thiol	Thiol-grafted Hyaluronic acid
MCF-7	Michigan Cancer Foundation-7
NHDF	Normal Human Dermal Fibroblasts
NHS	*N*-Hydroxysuccinimide
NIR	Near Infrared
ns	Non-significant
PBS	Phosphate Buffer Saline
PEG	Poly(ethylene glycol)
PI	Propidium Iodide
PTT	Photothermal therapy
rGO	Reduced graphene Oxide
ROS	Reactive oxygen species
S.D.	Standard Deviation

SEM	Scanning Electron Microscopy
Sulfo-SMCC	3-Sulfo-*N*-succinimidyl 4-(maleimidomethyl)-cyclohexane--1-carboxylate sodium salt
W/ NIR	With NIR laser exposure (808 nm, 1.7 W/cm^2)
W/o NIR	Without NIR laser exposure

Chapter 1

Introduction

1. Introduction

1.1. Cancer development, hallmarks, and treatments

1.1.1 Cancer

Cancer has been affecting humans for a long time and remains as one of the deadliest diseases in the world, being only surpassed by cardiovascular-related problems (1, 2). Worldwide, in 2020, 19.3 million new cancer cases were diagnosed, and there were approximately 10 million deaths as a consequence of this disease (1). In the United States of America, by the end of 2022, it is predicted the occurrence of an overwhelming 1,918,030 new cancer cases, of which 609,360 may be fatal (3). Despite the enormous efforts to prevent and treat cancer, the number of cases and deaths continues to rise rapidly. This data is a reminder that there should be a focus of scientific community in improving cancer-fighting therapies (1).

Cancer is a multifaceted set of diseases, characterized by a complex alteration of the cellular state, causing an uncontrolled and abnormal cellular growth that leads to destructive effects on the organism (4, 5). The causes for the development of a cancer cell are diverse. The main factors are genetic, where DNA mutations cause the loss of normal cellular functions. In addition, factors such as obesity, smoking, a sedentary lifestyle, advanced age, consumption of red meat, among others, have a huge contribute for the development of cancer cells (6-8).

These abnormal cells acquire new characteristics to sustain their uncontrolled proliferation. Over the years, several authors have proposed a set of hallmarks for cancer cells (Figure 1) (9). The hallmarks that are best accepted are those proposed by Hanahan and Weinberg, which have been subsequently refined by several authors (9, 10). These authors characterize cancer cells as having the following features: sustained proliferative signaling; evasion from growth suppressors; resistance to cell death; replicative immortality; angiogenesis inducers; activation of the invasion and metastasis process; reprogramming of energy metabolism; evasion from immune destruction; genomic instability; and tumor promoting inflammation (Figure 1) (10, 11). Most recently, with the help of various studies, new cancer features emerged as hallmarks, namely: the unlocking of a phenotypic plasticity and the presence of senescent cells. Additionally, two extra enabling characteristics emerged, which are: the non-mutational epigenetic reprogramming and the altered microbiome (9, 12).

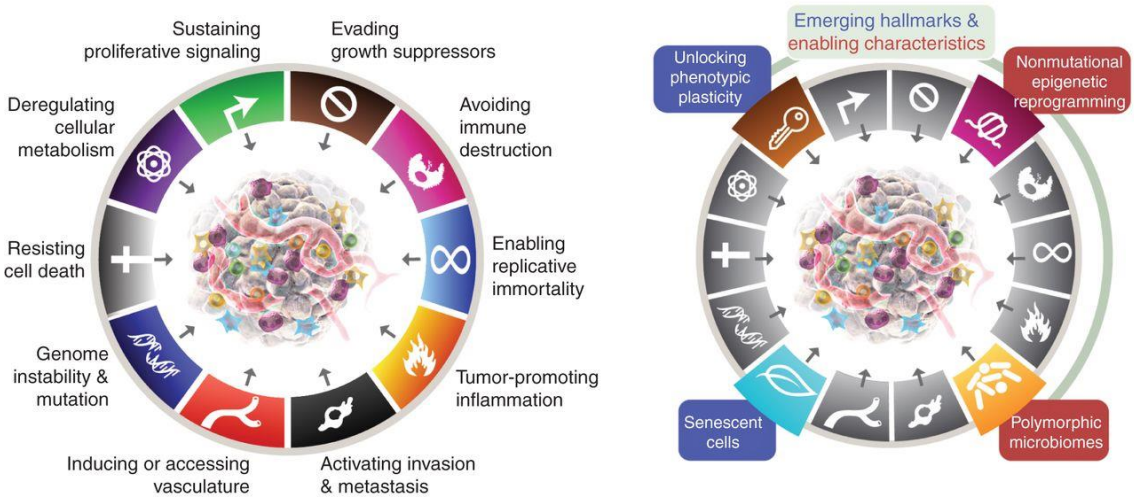

Figure 1: Cancer hallmarks proposed by Hanahan and Weinberg in 2011 (left): i) capacity to sustain proliferative signaling, ii) capacity to deregulate cellular metabolism, iii) resistance to cell death mechanisms, iv) induction of vasculature creation, v) activation of invasion and metastasis mechanisms, vi) replicative immortality, vii) avoidance of immune destruction, and viii) evasion to growth suppressors. The authors also proposed two enabling characteristics: i) genome instability and mutation, and ii) tumor-promoting inflammation. In 2022 (right), two new emerging hallmarks were proposed: i) the capacity to unlock phenotypic plasticity, and ii) the presence of senescent cells. Additionally, two new enabling characteristics were described: i) non-mutational epigenetic reprogramming, and ii) polymorphic microbiomes (Adapted from (12)).

Healthy cells are constantly replicating in order to maintain the structure and homeostasis of the tissues (11). This replication, encouraged through the production and release of growth factors, is normally controlled by several mechanisms (11). However, cancer cells have the ability to overcome these mechanisms by taking its own control (10, 11). These cells can, for example, segregate their own growth factors (10). Most of these factors have the ability to bind to cell receptors with tyrosine kinase activity, which regulates cell cycle progression and growth (10, 11). Cancer cells are also able to send signals to stimulate normal cells in the stroma to produce and supply them with growth factors (10, 11).

In order to maintain a state of "immortal" replication, cancer cells depend not only on growth factors, but also on cells' ability to escape the defenses, such as growth suppressors (10, 11). In a healthy tissue, irregular cell proliferation is controlled by these suppressors, acting as checkpoints over the replication cycle. There are several tumor suppressors, such as the Rb protein, the P53 pathway, and cyclin-dependent kinase inhibitors, that are prominent in cell division and cell cycle progression (10, 11, 13). However, cancer cells are able to bypass these defense mechanisms by downregulating the expression of these suppressor genes, thus having an open door for chronic proliferation (10, 11).

For sustaining chronic cell proliferation, cancer cells have the ability to resist cell death (10, 11). The most common approach is the loss of function on the protein P53, by suppression of the gene TP53, which serves as a critical cell damage sensor and initiator of apoptosis (10, 11, 13). The cancer cells can also bypass this defense by other methods, such as by overexpressing anti-apoptotic regulators (Bcl-2, Bcl-x_L) or by negative regulation of pro-apoptotic factors (Bax, Bim, Puma) (10, 11).

Additionally, cancer cells have an overexpression of the enzyme telomerase, which prolongs telomeric DNA at the ends of chromosomes. This limits the progressive erosion of telomeres, which creates a resistance to the induction of senescence/apoptosis, contributing to replicative immortality (10, 11). To further escape death, cancer cells are able to evade immune control mechanisms by sabotaging immune system checkpoints, overexpressing immune checkpoint inhibitors such as the programmed death protein-1, plus its ligands, and also inhibitors for the antigen 4, associated with cytotoxic T cells, an important asset of anti-tumor immunity (13, 14).

To ensure the supply of nutrients and oxygen for the exaggerated growth, cancer cells have the ability to stimulate the production of new blood vessels (angiogenesis) at a faster rate (10, 11, 13). Angiogenesis is stimulated by the upregulation of inducers like the vascular endothelial growth factor, which can occur through stimuli such as hypoxia, a characteristic of tumors, and remains activated continuously (10, 11, 13). With this abnormal and excessive growth, the vasculature tends to become aberrant, with several gaps, allowing more extravasation to the tumor site (10, 11, 13).

The cancer cells are also able to expand to different sites, activating the invasion and metastasis processes (10, 11, 13). This begins with cell invasion, followed by intravasation into the new aberrant vessels, and finally extravasation to new sites and growth of new malignant colonies, called metastases (10, 11, 13). Cell-cell and cell-to-extracellular matrix adhesion molecules are altered and help in the metastization process, such as the loss of E-cadherin and replacement by N-cadherin (10, 11, 13).

Cancer cells, being in a state of hyperproliferation, require more energy. They are able to reprogram their metabolism to utilize glucose by aerobic glycolysis rather than oxidative phosphorylation, to ensure a rapid energy demand and provide intermediates for anabolic reactions (10, 11, 13).

Additionally, the acquisition of many of the hallmarks comes from genomic alterations, due to mutations and chromosomal rearrangements, as well as loss of tumor suppressors and compromised DNA repair mechanisms (11, 15). These various alterations promote malignant transformation and facilitate tumor progression, providing ways for the tumor to overcome anti-tumor defense mechanisms (11, 15).

It is also well known that inflammatory conditions, especially chronic ones, increase the incidence of cancer, by supplying molecules such as growth or survival factors, among others (10, 11). The inflammatory microenvironment also assists the tumor development by releasing pro-tumorigenic cytokines and growth factors (10, 11). In addition, alterations in cellular metabolism and cofactors, such as S-adenosylmethionine, also link inflammation to cancer (10, 11, 13, 15).

In the last years, with the relentless research in this area, new hallmarks have emerged that help to better understand the complexity of cancer. It is now known that the microbiome can promote tumor formation and development, since some types of bacteria can cause DNA damage, inducing malformations in cells (9, 11, 12). Moreover, it was also proposed that the microbiome can exploit the inflammatory environment for a pro- or anti-tumor state (9, 11, 12).

Furthermore, cancer cells are able to unlock phenotypic plasticity, and differentiate back to a state similar to their progenitors and then follow an alternative pathway. They are also able to block differentiation, creating a continuous proliferation of partially differentiated cells (9, 12).

In addition to changes in the genome, growing evidence supports that cancer cells can evolve with purely epigenetic, non-mutational, changes (9, 12). This non-mutational epigenetic regulation is known to be the central mechanism mediating embryonic development, differentiation, and organogenesis, so disturbances in this system can lead to malformations at various cellular stages (9, 12).

Lastly, cellular senescence has long been seen as a protective mechanism against neoplasia (13, 15). However, the opposite has also been true, where sometimes senescent cells stimulate tumor development and malignant progression (13, 15). It has been demonstrated that senescent cancer cells contribute to proliferative signaling in various ways, such as preventing apoptosis, inducing angiogenesis, stimulating invasion and metastasis, and suppressing tumor immunity (13, 15).

1.1.2 Breast cancer

Breast cancer is a malignant disease that occurs in the mammary glands (16), and it is the most diagnosed cancer in women. Worldwide, 2,261,419 new cases and 684,996 deaths were reported for both genders in 2020 (1). This year, solely in the United States of America, 287,850 new cases of breast cancer in women are estimated to surge, corresponding to 31 % of all cancer types, with 43,250 associated fatalities (3). Although the survival rate is increasing, the existing treatments are quite invasive and painful, leaving permanent marks on the body, even if successful (1).

Breasts are constituted by lobules, ducts, fatty and fibrous connective tissue (17-19). The healthy breast duct consists of a layer of luminal epithelial cells surrounded by myoepithelial cells, which produce and attach to the basement membrane (Figure 2) (17, 18). The mammary microenvironment is composed by various types of stromal cells, including endothelial and immune cells, adipocytes, and fibroblasts, that produce the extracellular matrix, also a major component of the microenvironment (17, 18).

Numerous factors influence the onset of breast cancer. Factors such as age and hormones (linked to menopause or pregnancy), having poor lifestyle habits, or being exposed to carcinogenic substances, may contribute to cancer occurrence (20, 21). Genetic factors also play a central role in the development of these abnormalities, being notable the mutations in the genes BRCA1, BRCA2 or TP53 (16, 21, 22).

Breast cancer will appear when a variety of anomalies occur in breast cells (21, 23). Genetic mutations play an important role, such as the upregulation of oncogenes or mutations in genes involved in DNA repair (*e.g.* BRCA1), hence corrupting the cell homeostasis (21).

Breast cancer develops sequentially across defined stages, initiating with benign proliferative changes in the myoepithelial cells, leading gradually to their and the basement membrane destruction (Figure 2). Simultaneously, different cells like stromal fibroblasts, myofibroblasts, lymphocytes, and endothelial cells begin an atypical hyperplasia, forming a ductal carcinoma *in situ*. Upon the total destruction of the myoepithelial layer and basement membrane, the carcinoma evolves to an invasive state (17, 18, 24, 25).

If the disease continues to progress, the cancer cells can extravasate through the capillary wall to invade and colonize new areas of breast tissue, or even new areas of the body,

creating metastases (17, 18). Carcinoma-associated fibroblasts present in the area also play a role in tumor progression, as they promote tumor growth and increase tumor angiogenesis through paracrine signaling (17, 18). It's now known that tumor-associated macrophages facilitate angiogenesis, extracellular matrix degradation, and tumor invasion through activation of epidermal growth factor receptor signaling, protease secretion, and paracrine signaling between tumor cells (17, 18). Also worth mentioning is the fact that many chemokines are overexpressed in breast cancer cells (*e.g.* CXCL14), owing an important role in the tumor progression, such as cell proliferation, migration, and invasion (25).

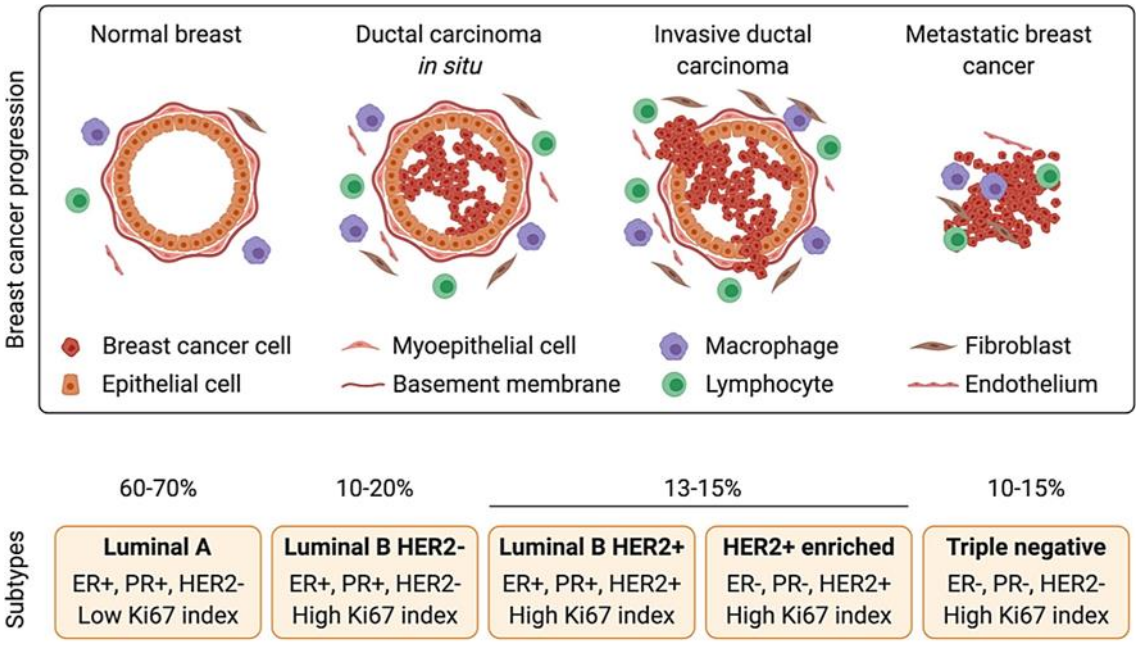

Figure 2: Illustrative representation of the progression of breast cancer microenvironment from homeostasis to metastatic stage. Healthy epithelial cells can suffer genetic or epigenetic alterations, leading to the origin of cancer cells in the breast tissue. While the epithelial cells decrease in number, the basement membrane is destroyed and the stromal cells increase, forming a ductal carcinoma *in situ*. With the basement membrane complete destruction, cancer cells can escape, evolving to an invasive state and subsequent metastization (Adapted from (26)).

With such complexity, different strategies of treatment are required. The breast cancer treatment is mostly chosen based on its stage at the time of diagnosis (23, 27-29). In the early stages, the preferred choice is breast-conserving surgery in combination with radiotherapy (23, 27-29). In more serious cases or in later stages, including the metastatic stage, it is recommended the use of systemic therapies, such as hormonal therapy, chemotherapy, targeted therapy, or any combination of these (23, 27-29).

However, the success of these therapies depends very much on the stage of the cancer, as well as the cancer and patient unique characteristics (23, 28, 29). Such treatments, even if successful, leave lifelong sequels in the patients since these are extremely invasive,

bringing complications such as pain, nausea, and permanent loss of the breasts (23, 30). Therefore, new, more effective, and less invasive forms of treatment have been sought to improve the quality of life of patients.

1.2. Nanomaterials mediated photothermal therapy

Nanomaterials have attracted a great interest for anticancer applications since the fine-tuning of their physicochemical properties (size, surface charge, and corona composition) can potentially enable their passive accumulation at the tumor site (31).

During the development of a nanostructure, the optimization of their size is an important step. Nanoparticles aimed for cancer therapy must not have a size lower than 5 nm, otherwise these can be easily cleared from blood circulation through renal filtration (32, 33). Additionally, nanoparticles with a diameter smaller than 50 nm usually accumulate in the liver, and thus are not able to reach the tumor site (32). On the other hand, if the nanomaterials' size exceeds 200 nm, these are most likely to get captured by macrophages or Kupffer cells, thus accumulating in the spleen and liver (32). Moreover, tumors' vasculature can have big fenestrations (ranging from 200 to 1200 nm), allowing these nanomaterials to extravasate and accumulate passively at the tumor site (34, 35). In addition, the tumor lymphatic system is usually compromised, not being able to remove the nanoparticles, further promoting nanoparticles' retention in this zone (36, 37). These two phenomena are known as the enhanced permeability and retention (EPR) effect. Considering this effect and the above-described size requirements, nanoparticles with sizes between 100 - 200 nm are often considered ideal for anticancer applications (34, 35).

Another aspect to take into consideration is the surface charge of the nanoparticles. It is known that highly charged nanoparticles, positively or negatively, are more likely to become opsonized or to suffer blood clearance by the cells of the reticuloendothelial system. Such events limit the nanostructures' blood circulation time and, consequently, diminish their probability to accumulate in the tumor by exploiting the EPR effect (38, 39). Therefore, neutral charged nanomaterials (zeta potential between - 10 and + 10 mV) are preferred in cancer therapy (38).

The corona of the nanoparticles, being the first point of interaction with the surrounding environment, also requires critical consideration. Biomolecules in the blood flow tend to adhere to the corona of the nanoparticles, changing their characteristics such as

immunogenicity, size and surface charge, thus affecting their accumulation at the tumor site (38). Additionally, the nanoparticles' corona also dictates their recognition by the body's defenses. It has therefore been explored how to functionalize and modify the nanoparticles' corona in order to increase their blood circulation time and targeting ability to cancer cells (38). For example, poly(ethylene glycol) (PEG) coatings make a barrier around the nanomaterials, protecting them from protein opsonization and reducing their clearance by the reticuloendothelial system, hence increasing the nanomaterials' blood circulation time as well as their biocompatibility (38). Moreover, specific molecules such as Hyaluronic Acid (HA), Folic acid or Transferrin, whose receptors are overexpressed in cancer cells, can be used to decorate the nanoparticles for achieving active targeting towards cancer cells (33, 39, 40).

Over the years, several types of nanomaterials have been developed for anticancer applications. In particular, photothermal nano-agents have been gathering a great interest. Following nanomaterials' internalization by cancer cells, usually occurring after intravenous administration and accumulation at the tumor site, the nanomaterials can perform different therapeutic modalities (41). In the specific case of photothermal nano-agents, these have the ability to interact with Near Infrared (NIR) light (750 – 1000 nm wavelength) (42). Upon irradiation of the tumor site with NIR light, these nanomaterials absorb the NIR radiation and convert it into heat, creating a temperature escalation (Photothermal Therapy (PTT)) that causes damage to cancer cells (Figure 3) (42).

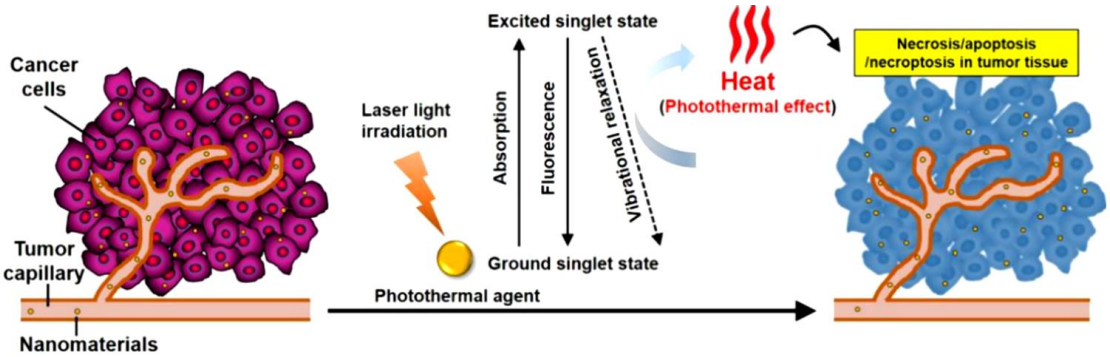

Figure 3: Schematic representation of PTT mediated by nanoparticles. Following nanoparticle administration and subsquente internalization into cancer cells, NIR light is directed into the tumor site for a specific period of time. The radiation is then converted into heat by the nanostructures, damaging the cancer cells depending on the temperature achieved (Adapted from (43)).

When the temperature rises to 41 – 45 °C, metabolic abnormalities are observed, damage is inflicted to the DNA and its repair systems, leaving the cells weakened and susceptible to elimination by the organism (44). In certain peripheral regions of the irradiated area, there is an increase in reactive oxygen species (ROS), which may lead to oxidative stress

(44, 45). In some cases, this kind of sublethal damage provokes the release of pro-inflammatory molecules such as cytokines (*e.g.* IL-1β), stimulating the action of immune cells (44, 46). As temperature rises above 50 °C, the effects become irreversible and lethal (44, 46). At this temperature (or above), proteins start to denature, inactivating vital enzymes for cells such as DNA polymerase, and thus breaking down DNA replication (44, 46). The cell membrane eventually begins to collapse, lysosomal degrading enzymes are released, and the Golgi complex and mitochondria deteriorate (44, 46). Finally, cells can also experience necrosis (Figure 4) (45, 47, 48).

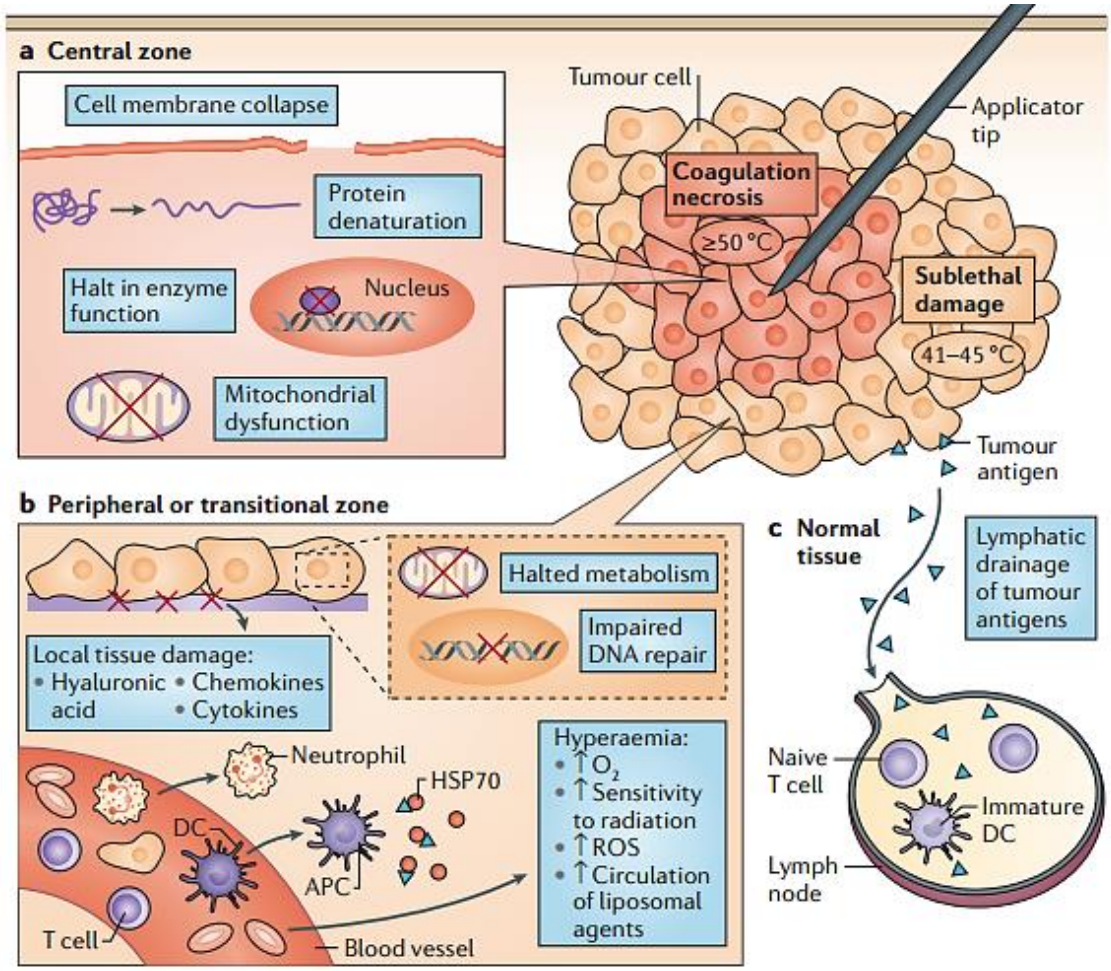

Figure 4: Illustration of the temperature effects on cancer cells. Therapeutic effects start around 41 °C, with sublethal damage such as an increase in ROS or DNA damage. When temperature reaches temperatures above 50 °C, irreversible damage occurs, and the cancer cells might experience necrosis (Adapted from (44)).

When using photothermal nano-agents for cancer therapy, utilizing NIR light is extremely helpful, since it displays high penetration in biological tissues and few interaction with the surrounding biomolecules (*e.g.* collagen, lipids, hemoglobin or water), reaching closely 2 cm of penetration depth (42, 44).

Various materials have been used to develop nano-agents for PTT. A popular strategy relies on the encapsulation of NIR-absorbing small molecules (*e.g*. Indocyanine green, IR780, IR820) in nanomaterials (49). In general, the photothermal nano-agents produced by this strategy have a greater biocompatibility but present a low photothermal conversion efficiency and weak photostability (43). In turn, inorganic photothermal nano-agents have superior optical properties but may require additional modifications to display suitable biological properties and their synthesis may be laborious. For instance, gold nanorods have been widely explored in the last years because of their good optical properties. However, attaining nanorods with a strong NIR absorption is not a straightforward synthesis and purification process (47). Therefore, new materials are required for cancer PTT, and those based on Graphene Oxide (GO) and its reduced form have been showing promising results (50).

1.2.1 Graphene based nanomaterials for cancer PTT

GO is a 2D nanomaterial with a graphitic structure that incorporates oxygen-functional groups (*e.g*. carboxyl, hydroxyl and epoxy groups) (Figure 5) (51). In the recent years, GO has gathered a lot of interest for cancer therapy due to its i) ability to encapsulate molecules (*e.g*. chemotherapeutic drugs) through hydrophobic-hydrophobic interaction or π-π stacking, and ii) great interaction with NIR light, generating a photothermal effect (38, 50, 52). In order to improve GO's therapeutic potential, this nanomaterial can be reduced, generating reduced GO (rGO). The reduction process can occur through chemical, thermal, or electrical methods (53). Upon its reduction, the oxygen functional groups are removed (Figure 5), improving the materials' loading capacity and, most importantly, their NIR absorption/photothermal capacity (51, 52, 54).

Figure 5: Schematic representation of the reduction of GO.

To obtain rGO, usually chemical methods are used, in which the most common reducing agent is hydrazine hydrate (34, 38). However, this agent grants cytotoxicity to the obtained rGO nanomaterials, restraining its clinical use (51). Consequently, alternative reduction methods with green reducing agents are becoming popular, such as those based on L-ascorbic acid, L-cysteine and dopamine (51, 52, 54). In this regard, Lima-Sousa and co-workers recently optimized a novel method to produce rGO by using

dopamine (termed as DOPA-rGO). This rGO derivative displayed an improved NIR absorption/photothermal capacity, good cytocompatibility and water solubility (55).

In some cases, PTT alone is not enough to completely eradicate de tumor, due to the dissimilar tumor architecture, which can lead to an uneven heat distribution (56). In order to maximize the therapeutic outcome, the use of a combinatorial therapy can be advantageous. In this regard, the aromatic lattice of DOPA-rGO can be used to encapsulate hydrophobic chemotherapeutic drugs (57, 58), enabling its use in cancer chemo-PTT. Moreover, the nanomaterials' photoinduced heat can trigger the release of drugs, contributing to an on-demand therapeutic effect (57, 59).

There are some hurdles regarding DOPA-rGO nanomaterials, and nanostructures in general, that must be surpassed to enable their translation (Figure 6). While DOPA-rGO has adequate water solubility, its stability in biological fluids needs to be improved. Nanoparticles in general face numerous biological barriers following their systemic injection, which affect their tumor-homing capacity (60). Before reaching the tumor, nanoparticles often encounter phagocytic cells who sequester them, restraining their distribution (60-62). This limitation has been addressed by functionalizing the nanostructures' surface with PEG or poly(2-oxazolines) (63, 64). These coatings can also prevent protein adsorption, avoiding nanoparticles' opsonization (63, 65). Other problems also arise when designing nanoparticles that are intended to achieve tumor uptake using only the EPR effect. Some studies have shown that the EPR effect is not ubiquitously present in all human solid tumors and that additional mechanisms also govern the nanoparticles' tumor accumulation (*e.g.* dynamic vents, active transport through endothelial cells) (66, 67). Moreover, nanoparticles can also struggle to penetrate into the tumor tissue due to the high interstitial fluid pressure in this zone (60-62). Peculiarly, a recent study reported that only 0.7 % of the intravenously injected nanoparticles' dose reaches the tumor (60). Considering all of these constrains, it is fundamental to investigate novel technologies to deliver nanomaterials into the tumor that are not affected by the systemic administration issues.

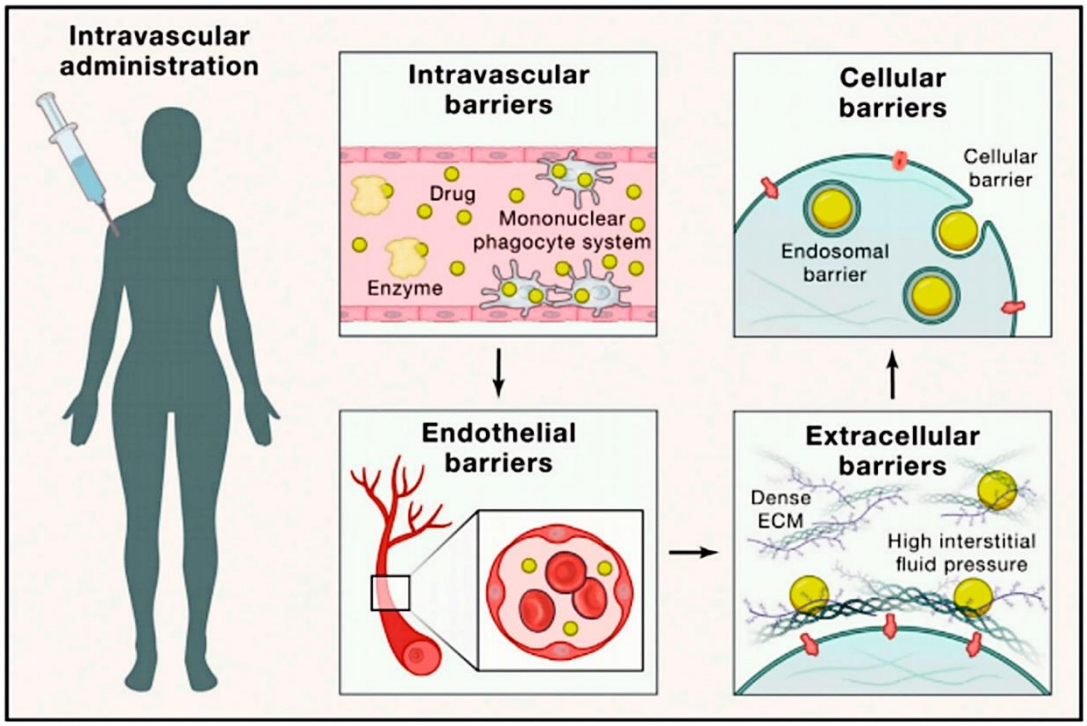

Figure 6: *S*chematic representation of some biological barriers that affect the tumor-homing capacity of systemically administered nanoparticles (Adapted from (68)).

1.3. Hydrogels for localized cancer therapy

Locally administered macro-scale delivery systems are emerging to address the limitations associated with the intravenous administration of the nanomaterials (69, 70). These macro-systems act as nanoparticles' reservoirs, facilitating their sustained delivery at the tumor site (Figure 7) (70). Additionally, these macro-scale delivery systems have the ability to protect the therapeutic agents from the body's defenses (70). By mediating a direct delivery of the nanoparticles in the tumor zone, these macro-systems enable the usage of lower nanoparticle dosages (70).

Several types of macro-scale systems are being developed, with hydrogels and micro-needles being the most prominent (69). Micro-needles, which are structures capable of piercing the skin, are prime systems for subcutaneous delivery of therapeutic agents/nanoparticles. In this way, their use is restricted to the treatment of superficial cancers (69). In turn, hydrogels are a three-dimensional hydrophilic crosslinked polymeric network that can be administered in deeper regions, as they are usually implanted or administered through a syringe, allowing the local delivery of nanostructures entrapped in their porous structure (71, 72).

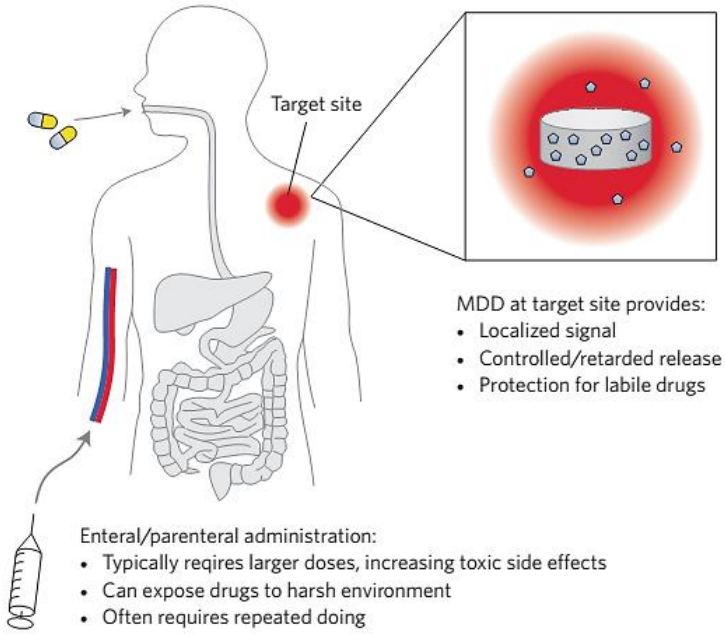

Figure 7: Illustration depicting the limitations of systemic delivery and the advantages of using macro-scale delivery devices (Adapted from (70)).

Hydrogels containing nanomaterials can be applied in cancer therapy through two different ways. In one approach, the hydrogel precursor solution (*e.g*. polymers, crosslinking agents) and the nanomaterials are loaded into a syringe and, after administration at the tumor site, the hydrogels are formed *in situ*. In the other strategy, the hydrogel can be pre-formed and posteriorly implanted into the body (*e.g*. for postoperative therapy) (73). Hydrogels can be assembled through a myriad of crosslinking reactions (74). In what concerns non-covalent interactions, the ionotropic gelation has been a popular mechanism explored to attain hydrogels (74, 75). In turn, covalent interactions, such as photo-crosslinking reactions, Michael type addition, and Schiff base reactions have also been used to produce hydrogels (73, 76, 77).

So far, various types of hydrophilic materials have been studied in the assembly of hydrogels (73, 76, 77). Natural polymers (such as HA, Alginate, Dextran) are preferred due to their biocompatibility and biodegradability (73, 76, 77). In turn, synthetic materials (such as PEG or poly(acrylamide)) have stronger mechanical properties and are easily fine-tuned (73, 76, 77).

1.4. Engineering covalently crosslinked implantable hydrogels for cancer photothermal therapy

Implantable hydrogels can provide an accurate and tumor-confined delivery of therapeutics, including photothermal nano-agents, ensuring high dosages at the target site with minimal exposure to healthy tissues (71, 78). Considering that implantable hydrogels are pre-formulated (*i.e.,* these are assembled outside the body), they can offer an immediate therapeutic action upon implantation and can be tailored to fit the implantation site (71, 79, 80).

Covalently crosslinked hydrogels are mechanically stronger, thus avoiding early degradation and, consequently, diminishing the concerns regarding a premature release of the nanomaterials (73). Furthermore, their porous structure and gelation time are less variable, allowing a more consistent performance (74). In this way, a prolonged and tumor-confined nanoparticle delivery can be achieved (73).

In particular, hydrogels assembled through Michael-type addition reaction display suitable features, such as high efficiency of crosslinking, regioselectivity and are also formulated under mild conditions (*e.g.* using water as a solvent) (74, 81, 82). Michael-type addition reactions usually take place between a nucleophile (Michael donors), like amines or thiols groups, and an α, β-unsaturated carbonyl containing compound (Michael acceptors), such as ketones or maleimides (81, 83, 84).

From the many possible combinations, Thiol-Maleimide Michael-type additions present a great selectivity between maleimides and thiol groups, as well as rapid crosslinking (85, 86). Despite their advantages, most of the Thiol-Maleimide crosslinked hydrogels employ synthetic polymers (*e.g.* PEG-Thiol, PEG-Maleimide), which is not optimal considering their poor biodegradability.

In this way, it is crucial to design Thiol-Maleimide implantable hydrogels using natural polymers due to their excellent biocompatibility and biodegradability. Chitosan (Ch), a polysaccharide derived from the *N*-deacetylation of chitin, is a natural polymer fairly used for hydrogels formulation due to its good biocompatibility, biodegradability and antibacterial properties (72, 87). It is possible to further deacetylate chitosan (dCh) (88), improving the availability of primary amine groups. The primary amines of dCh can react with different molecules in order to include Maleimide functional groups in its structure (89, 90).

HA is a natural polymer formed in the extracellular matrix (91-93). This glycosaminoglycan has good biocompatibility, biodegradability and very low immunogenicity (92, 93). Even though HA can be used for building hydrogels using non-covalent ionotropic interactions, these are quickly degraded (92, 93). In this regard, the thiolation of HA opens a venue for its use in the assembly of Thiol-Maleimide hydrogels (94).

Overall, developing an implantable hydrogel based on the Thiol-Maleimide crosslinking, using Maleimide-grafted dCh (dCh-Mal) and Thiol-grafted HA (HA-Thiol), for the delivery of drug-loaded DOPA-rGO is a never explored approached with good potential for combinatorial breast cancer chemo-PTT.

Chapter 2

Aims

Aims

The main aim of this Master Thesis work plan was to produce a novel Thiol-Maleimide crosslinked hydrogel, based on HA-Thiol and dCh-Mal, incorporating DOPA-rGO loaded with Doxorubicin (DOX/DOPA-rGO), for application in the combinatorial chemo-PTT of breast cancer cells.

The specific aims of this Master Dissertation plan are:

- Synthesis and characterization of dCh-Mal, HA-Thiol, DOPA-rGO and DOX/DOPA-rGO;
- Formulation of the Thiol-Maleimide HA-Ch based hydrogels;
- Characterization of the physicochemical and photothermal properties of the hydrogels;
- Determination of the cytocompatibility of the HA-Ch based hydrogel loaded with DOPA-rGO;
- Evaluation of the PTT mediated by HA-Ch based hydrogel loaded with DOPA-rGO against breast cancer cells;
- Investigation of the chemo-PTT mediated by HA-Ch based hydrogel loaded with DOX/DOPA-rGO towards breast cancer cells.

Chapter 3

Experimental Section

3. Experimental Section

3.1. Materials

Ch (medium molecular weight), GO nanocolloids, *N*-Hydroxysuccinimide (NHS), Cysteine, Dulbecco's Modified Eagle's Medium F-12 (DMEM-F12), Resazurin, Phosphate Buffered Saline (PBS), Fetal Bovine Serum (FBS) and Penicillin/Streptomycin were acquired from Sigma-Aldrich (Sintra, Portugal). 3-Sulfo-*N*-succinimidyl 4-(maleimidomethyl)-cyclohexane-1-carboxylate sodium salt (Sulfo-SMCC), Propidium Iodide (PI) and Lysozyme from chicken egg were purchased from Alfa Aesar (Lancashire, UK). Methanol and T-flasks were bought from Thermo Fisher Scientific (Porto, Portugal). Dopamine hydrochloride was obtained from Acros Organics (New Jersey, USA). Calcein-AM was obtained from Merck Milipore (Algés, Portugal). NaOH was acquired from LabChem (Pennsylvania, USA). DOX and HA (extra low molecular weight) were gotten from Carbosynth (Berkshire, UK). 1-Ethyl-3-(3-dimethylaminopropyl) carbodiimide (EDC) was obtained from Calbiochem (Darmstadt, Germany). Michigan Cancer Foundation-7 (MCF-7) cell line was provided by ATCC (Middlesex, UK). Normal Human Dermal Fibroblasts (NHDF) were supplied from PromoCell (Heidelberg, Germany). Cell culture plates were acquired from VWR (Alfragide, Portugal). The water used in the entire work was double deionized (0.22 μm filtered; 18.2 MΩ cm).

3.2. Methods

3.2.1. Synthesis and characterization of dCh-Mal and HA-Thiol

The production of dCh-Mal was accomplished using a two-step process based on the deacetylation of Ch and its subsequent reaction with Sulfo-SMCC. Initially, the deacetylation of Ch was accomplished as previously described by Gaspar *et al.* with minor modifications (95). In brief, Ch was mixed with NaOH, and it was allowed to react for 3 h at 50 °C under stirring. Then, this solution was washed with water, vacuum filtered and freeze-dried, yielding dCh. Subsequently, Sulfo-SMCC was reacted with dCh according to the protocol described by El-Sayed *et al.* with minor modifications (90). In brief, dCh and Sulfo-SMCC were dissolved in PBS at pH 7.5. This mixture was left to react for 24 h under stirring at room temperature. The obtained product was then dialyzed against water for 3 days (14 kDa molecular weight cut-off membrane), yielding dCh-Mal.

The synthesis of HA-Thiol was performed as previously described by Sousa *et al.* (96), with minor adaptations. Briefly, an aqueous solution of HA, EDC and NHS was prepared. The resultant solution pH was then adjusted to 5.5, and subsequently left to react for

30 min under stirring at room temperature. Afterwards, an aqueous solution of Cysteine was added to the previous mixture, being left to react for 4 h under stirring at room temperature. This final solution was dialyzed against water for 3 days (14 kDa molecular weight cut-off membrane), yielding Thiol-grafted Hyaluronic acid (HA-Thiol).

The successful synthesis of dCh, dCh-Mal and HA-Thiol were confirmed by Fourier-Transform Infrared (FTIR) spectroscopy, using a Nicolet iS10 spectrometer (ThermoScientific Inc., MA, USA). These polymers were also characterized by Proton nuclear magnetic resonance (^{1}H NMR) using a Brüker Avance III 400 MHz spectrometer (Brüker Scientific Inc., NY, USA). For this purpose, dCh (30:1 (v/v) D_2O/HCl 1 M), dCh-Mal (30:1 (v/v) D_2O/HCl 1 M), HA (9:1 (v/v) H_2O/D_2O), Cysteine (9:1 (v/v) H_2O/D_2O), and HA-Thiol (9:1 (v/v) H_2O/D_2O) were analyzed at 298 K. The spectra obtained were analyzed in MestReNova software (Mestrelab Research, SL, Santiago de Compostela, Spain).

3.2.2. Synthesis and characterization of DOPA-rGO and DOX/DOPA-rGO

The synthesis of DOPA-rGO was performed according to the method previously described by Lima-Sousa *et al.* (55). Before its use, GO was firstly sonicated for 6 h. Following this step, Dopamine hydrochloride was added to the GO solution and the reaction was carried out under stirring at 60 °C and pH 8.5 (adjusted using NaOH) for 4 h. The synthesized material was then purified by dialysis against water for 2 h (14 kDa cut-off dialysis membrane), yielding DOPA-rGO. Then, DOX was encapsulated into DOPA-rGO by a simple sonication process (97). In brief, an aqueous solution of DOPA-rGO and DOX were sonicated for 30 min in an ultrasonic bath, yielding DOX/DOPA-rGO.

The size distribution of DOPA-rGO and DOX/DOPA-rGO was evaluated with Dynamic Light Scattering (DLS) in a Zetasizer Nano ZS (Malvern Instruments Ltd., Worcestershire, UK). The NIR absorption capacity of these materials was also explored trough Absorption spectroscopy, using an Evolution 201 spectrophotometer (Thermo Scientific Inc., MA, USA).

3.2.3. Formulation and characterization of the Thiol-Maleimide HA-Ch based hydrogels

The assembly of Thiol-Maleimide HA-Ch implantable hydrogels incorporating DOX/DOPA-rGO was performed according to the protocol by Matsumoto *et al.* with minor modifications (89). Briefly, DOX/DOPA-rGO, HA-Thiol and dCh-Mal were mixed

in round-bottom microtubes for attaining hydrogels with similar macroscopic properties for all the assays – abbreviated as DOX/DOPA-rGO@TMgel. After complete crosslinking, the formulations were recovered by gentle centrifugation and stored at 4 °C before their use. For the formulation of the Thiol-Maleimide HA-Ch based hydrogels incorporating DOPA-rGO (abbreviated as DOPA-rGO@TMgel), the same protocol was employed using DOPA-rGO. As control, formulations i) without Maleimide groups (*i.e.,* prepared using dCh, HA-Thiol and DOPA-rGO) and ii) without Thiol groups (*i.e.,* prepared using dCh-Maleimide, HA and DOPA-rGO) were also produced.

The gelation of the produced hydrogels was confirmed by the inverted microtube method (98). The superficial and inner (cross-section) morphologies of the hydrogels were observed by Scanning Electron Microscopy (SEM) operated at an acceleration voltage of 20 kV (Hitachi S-3400N Scanning Electron Microscope, Japan). To visualize the degradation of the DOX/DOPA-rGO@TMgel and DOPA-rGO@TMgel in physiological-like conditions, these were immersed in PBS (pH 7.4) supplemented with Lysozyme (13.6 mg/L) and incubated at 37 °C under stirring for 7 days. Then, the hydrogels were recovered, washed with water, freeze-dried, and imaged by SEM as described above.

To assess the long-term stability of hydrogels, all the individual precursor solutions (*i.e.,* those containing dCh-Mal, HA-Thiol, DOPA-rGO or DOX/DOPA-rGO) were prepared and stored at 4 °C for 7 days. Afterwards, these aged precursor solutions were used to assemble the hydrogels, and their gelation was confirmed by the inverted microtube test. Additionally, DOPA-rGO and DOX/DOPA-rGO size distribution and NIR absorption after storage (for 7 days at 4 °C) were also assessed.

The photothermal capacity of DOX/DOPA-rGO@TMgel and DOPA-rGO@TMgel was investigated as previously described by Lima-Sousa *et. al.* (51). In brief, these formulations were placed in water and irradiated with NIR light (808 nm, 1.7 W/cm^2) for 10 min. The temperature variations (ΔT) were recorded by using a thermocouple thermometer. As a control, the temperature change of water (without hydrogels) was also measured.

3.2.4. *In vitro* evaluation of the cytocompatibility of the DOPA-rGO@TMgel

To evaluate the cytocompatibility of DOPA-rGO@TMgel, this formulation was placed in contact with models of healthy (NHDF) and breast cancer (MCF-7) cells (98). Briefly, a density of 2 x 10^4 cells/well was seeded in 24-well plates in DMEM-F12 medium supplemented with 10 % FBS and 1 % Penicillin/streptomycin and cultured in a

humidified incubator (at 37 °C; 5 % CO_2). After 24 h of cells' growth, these were incubated with the DOPA-rGO@TMgel (in fresh culture medium) for 24 h and 48 h. Afterwards, the hydrogels were removed from the wells, the medium was replaced with fresh medium containing resazurin (10 % (v/v)) and the cells were incubated for 4 h in the dark (at 37 °C; 5 % CO_2). Cell viability was assessed after the incubation period by reading the fluorescence of the Resorufin (λ_{ex} = 560 nm, λ_{em} = 590 nm) in a Spectramax Gemini EM spectrofluorometer (Molecular Devices LLC, USA) (99). In addition, cells were also incubated with only culture medium or ethanol (70 % (v/v)), being the negative (K^-) or positive (K^+) controls, respectively.

3.2.5. *In vitro* evaluation of the PTT mediated by DOPA-rGO@TMgel and chemo-PTT mediated by DOX/DOPA-rGO@TMgel

The DOPA-rGO@TMgel' and DOX/DOPA-rGO@TMgel' phototherapeutic potential against breast cancer cells was assessed using the resazurin method (98). For such, the same cell density of MCF-7 cells described in 3.2.4. was cultured and, after 24 h, these were incubated with DOPA-rGO@TMgel or DOX/DOPA-rGO@TMgel (in fresh culture medium). Four hours later, the hydrogels were exposed to NIR light (808 nm, 1.7 W/cm^2) for 10 min. Upon reaching 24 h of incubation with the hydrogels, the cells were incubated with resazurin, and their viability determined as described in section 3.2.4.

In order to obtain visual confirmation of the therapeutic effect of DOPA-rGO@TMgel and DOX/DOPA-rGO@TMgel, MCF-7 cells were first seeded and incubated with these formulation as described above (98). After 4 h, the hydrogels were irradiated with NIR light (808 nm, 1.7 W/cm^2, 10 min), and the cells were stained with Calcein-AM/PI (used to label live/dead cells, respectively) according to the manufacturer's protocol. Fluorescence images were acquired by Confocal Laser Scanning Microscopy (CLSM; Zeiss LSM 710, Carl Zeiss AG, Oberkochen, Germany) using a $\lambda_{ex}/\lambda_{em}$ of 488/493–556 (Calcein-AM) and 561/566–719 nm (PI) (97). Non-irradiated cells exclusively incubated with culture medium were considered the control for live cells.

3.2.6. Statistical analysis

For multiple groups comparison, a one-way Analysis of Variance (ANOVA) was applied with the Student-Newman-Keuls test. A *p*-value lower than 0.05 ($p < 0.05$) was deemed statistically significant. All data are represented as the mean ± standard deviation (S.D.). Data analysis was achieved using the software GraphPad Prism v6.0 (Trial version, GraphPad Software, CA, USA).

Chapter 4

Results and Discussion

4. Results and Discussion

4.1. Synthesis and characterization of dCh-Mal, HA-Thiol and DOX/DOPA-rGO

Prior to the assembly of the novel natural polymer-based Thiol-Maleimide implantable hydrogel incorporating DOX/DOPA-rGO (DOX/DOPA-rGO@TMgel) aimed for cancer chemo-PTT (Figure 8), polymers (dCh-Mal and HA-Thiol) compatible with this crosslinking chemistry were prepared. Parallelly, DOPA-rGO was also produced and then loaded with DOX.

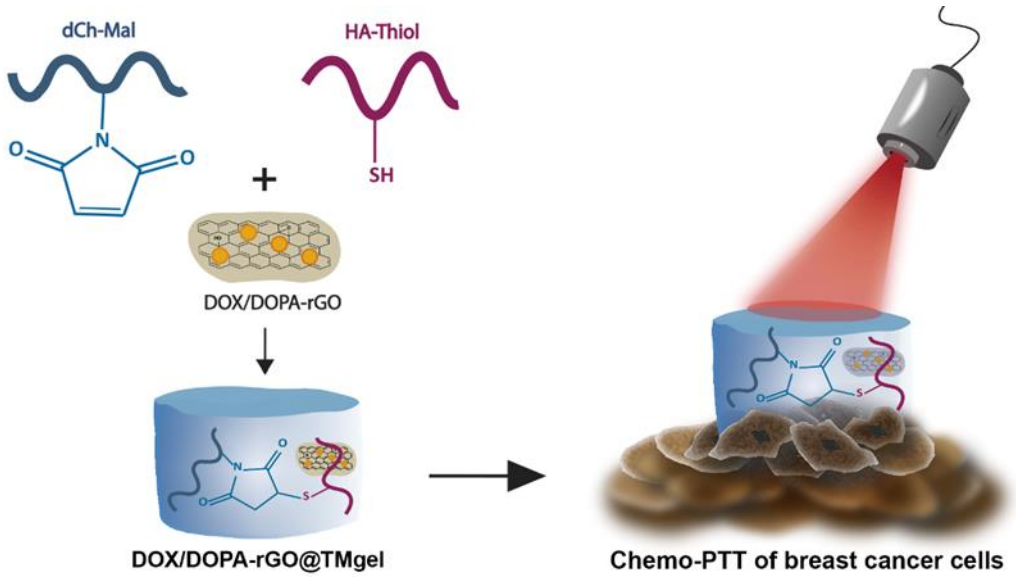

Figure 8: Illustration of the formulation of the Thiol-Maleimide based implantable hydrogel incorporating DOX/DOPA-rGO, and its use in the chemo-PTT of breast cancer cells.

The synthesis of dCh-Mal was performed in a two-step process – Figure 9. First, Ch was deacetylated to increase the available NH_2 groups (95), hence facilitating the subsequent binding of the Sulfo-SMCC (contains the Maleimide groups) (90), yielding dCh-Mal. The successful synthesis of dCh was confirmed by FTIR spectroscopy – Figure 10A and 10B. The FTIR spectrum of Ch presents peaks at 3354 cm^{-1} (O-H stretch) and 3290 cm^{-1} (N-H stretch) from the chemical groups present on the *N*-Acetylglucosamine/Glucosamine rings as well as peaks at 1647 cm^{-1} (C=O stretch) from its *N*-acetyl group and 1567 cm^{-1} (N-H bending) from its primary amines (100) – Figure 10A. The FTIR spectrum of dCh also presented these peaks (Figure 10A). However, the intensity of the peak at 1647 cm^{-1} (C=O stretch) decreased and that at 1567 cm^{-1} (N-H bending) increased (Figure 10B), indicating the removal of

the *N*-acetyl groups and formation of primary amines, respectively (100). Taken together, this data confirms the successful synthesis of dCh.

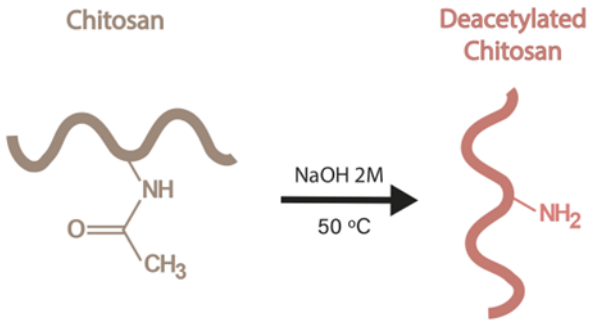

Figure 9: Schematic representation of the deacetylation of Ch.

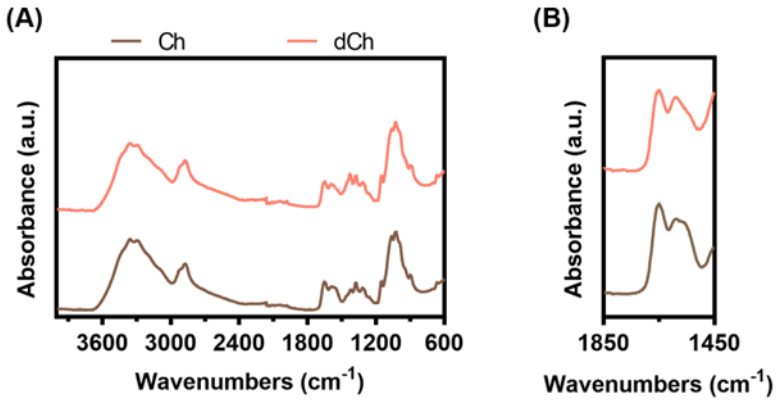

Figure 10: FTIR spectra of Ch and dCh (A). FTIR spectra of Ch and dCh in the 1850-1450 cm^{-1} wavenumber range (B).

Afterwards, dCh was reacted with Sulfo-SMCC in order to attain dCh-Mal (90) – Figure 11. The FTIR analysis revealed that the dCh-Mal displayed the dCh typical peaks (Figure 12). The dCh-Mal spectrum appeared to have a higher intensity in its 1643 cm^{-1} peak (C=O stretch). Moreover, its spectrum also displayed a peak at 1257 cm^{-1} (C-N stretch), which is also presented on Sulfo-SMCC FTIR data.

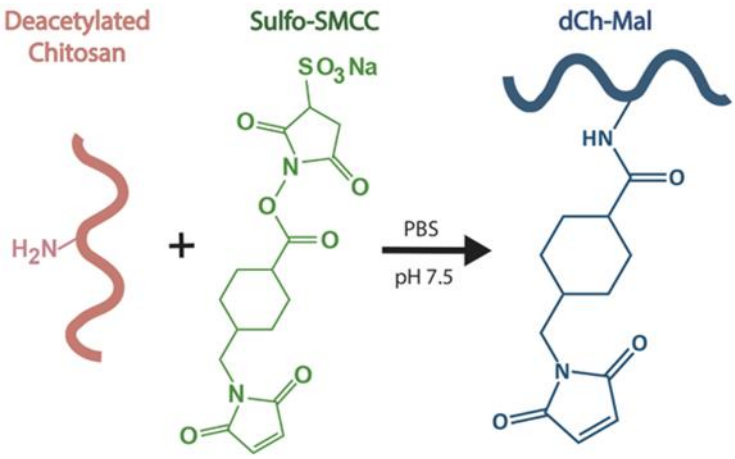

Figure 11: Schematic representation of the reaction between dCh and Sulfo-SMCC.

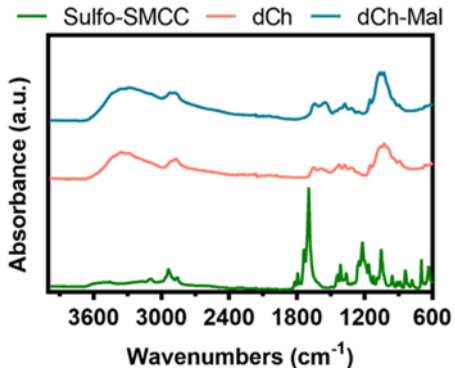

Figure 12: FTIR spectra of Sulfo-SMCC, dCh and dCh-Mal.

Then, ^{1}H NMR analysis was employed to prove the dCh-Mal synthesis (Figure 13). The ^{1}H NMR spectra of dCh and dCh-Mal displayed peaks at δ ≈ 3.1 ppm (-C**H** from the C-2 of the glucosamine unit) and δ ≈ 4.0 - 3.5 ppm (-C**H** from the pyranose ring) (101-103). As importantly, the ^{1}H NMR spectrum of dCh-Mal also presented the signature peaks of bonded Sulfo-SMCC (Figure 11), namely at δ ≈ 1.6 - 1.1 ppm (-C**H₂** from Sulfo-SMCC cyclohexane) and δ ≈ 6.3 ppm (C**H**=C**H** of Maleimide) (90, 103, 104).

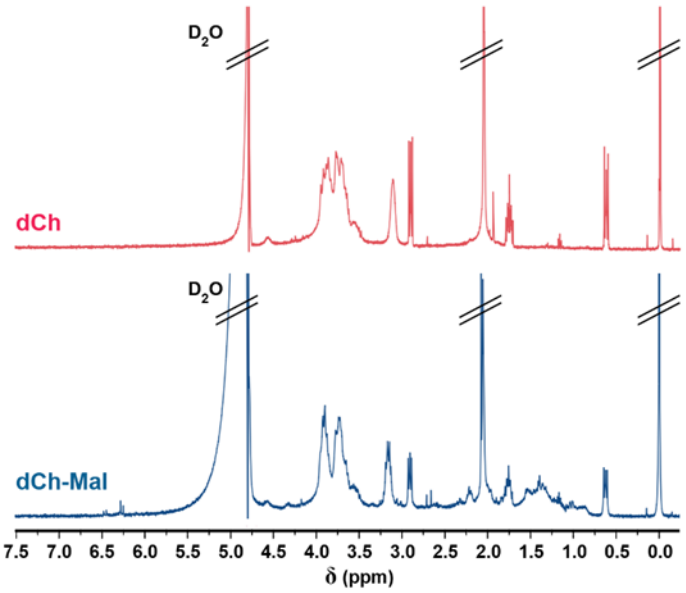

Figure 13: ^{1}H NMR spectra of dCh and dCh-Mal.

In turn, to prepare HA-Thiol, HA and Cysteine were reacted using the carbodiimide chemistry (96) – Figure 14. The FTIR spectrum of HA presented several signature peaks such as 3290 cm^{-1} (O-H and N-H stretches) and 1607 cm^{-1} (C=O stretch) – Figure 15A (105). The FTIR spectrum of Cysteine presented peaks at 2551 cm^{-1} (S-H stretch) and 1574 cm^{-1} (N-H bending). The FTIR spectrum of HA-Thiol presented the HA and Cysteine signature peaks (Figure 15A and 15B), as well as a peak with an increased intensity at 1557 cm^{-1} (N-H in secondary amides) (106).

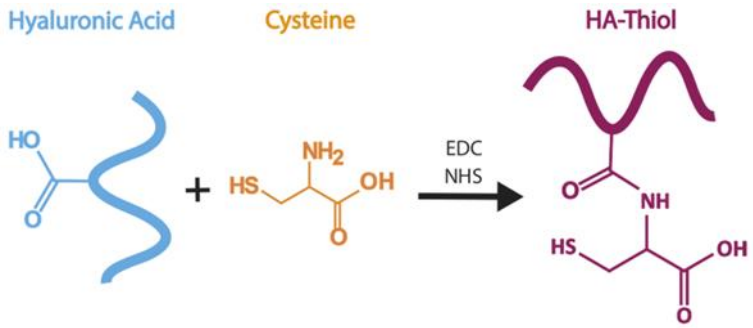

Figure 14: Schematic representation of the preparation of HA-Thiol.

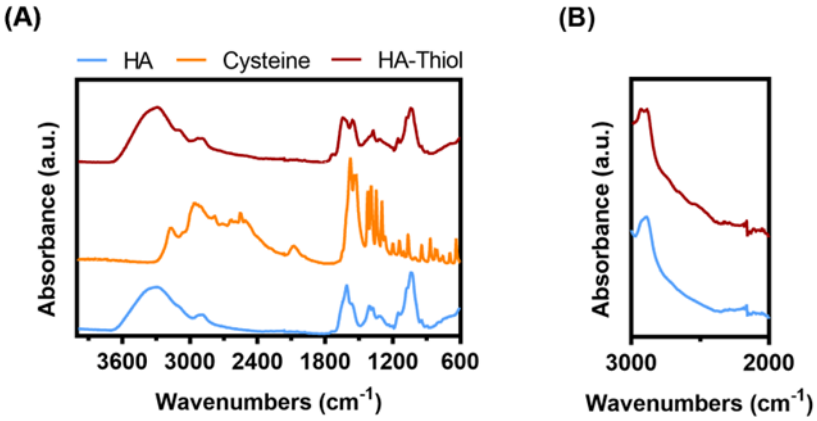

Figure 15: FTIR spectra of HA, Cysteine and HA-Thiol (A). FTIR spectra of HA and HA-Thiol in the 3000-2000 cm^{-1} wavenumber range (B).

Further, ^{1}H NMR analysis was employed to confirm HA-Thiol synthesis (Figure 16). The NMR spectrum of HA presented peaks at δ ≈ 2.0 ppm (-C**H**$_3$; acetyl group protons), δ ≈ 3.9-3.2 ppm (-C**H**$_2$ and -C**H** protons from the sugar ring) and δ ≈ 4.6-4.4 ppm (-C**H** from anomeric protons) (51). On the other hand, the NMR spectrum of Cysteine displayed peaks at δ ≈ 3.1-3.0 ppm (-C**H**$_2$) (107). In turn, the HA and Cysteine signature peaks could be observed on the spectrum of HA-Thiol, hence confirming its successful preparation.

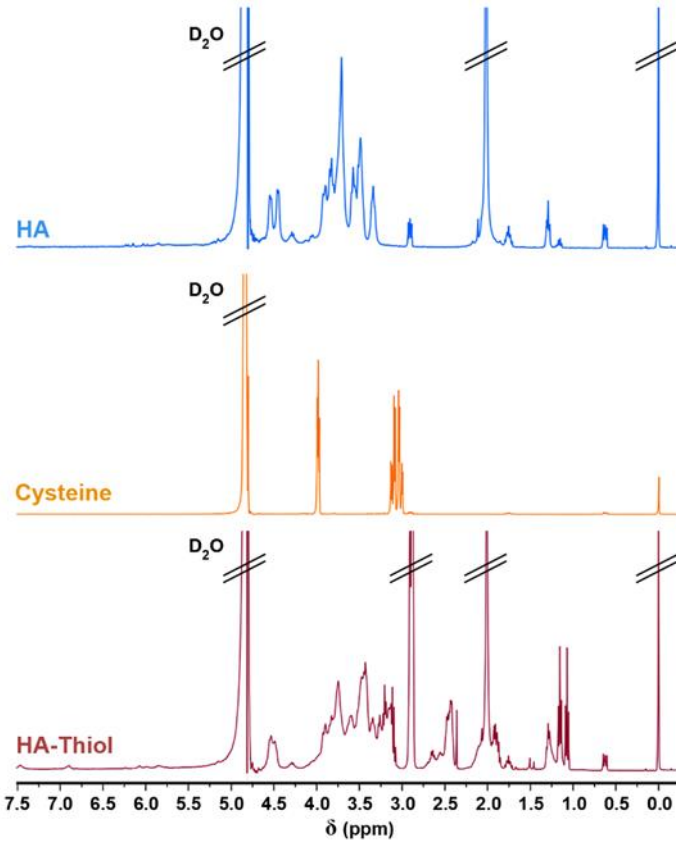

Figure 16: ^{1}H NMR spectra of HA, Cysteine and HA-Thiol.

By last, the reduction reaction of GO was achieved using Dopamine as the reducing agent (55). Afterwards, DOPA-rGO was loaded with DOX using a simple sonication process (97). The DLS analysis showed that DOPA-rGO and DOX/DOPA-rGO have a size distribution within the range considered optimal for cancer related applications (108) – Figure 17A and 17C. Absorption spectroscopy data also revealed that both nanomaterials have a high NIR absorption (Figure 17B and 17D), which is crucial for enabling their use in photothermal applications (109).

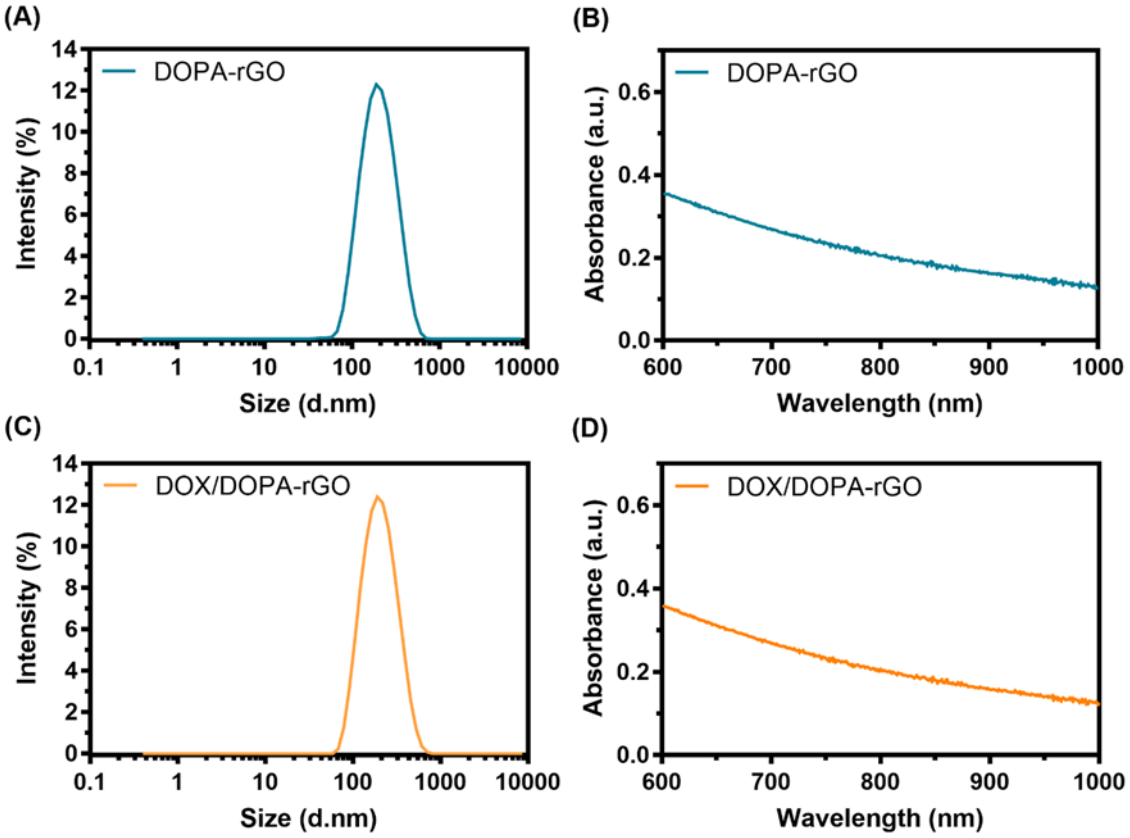

Figure 17: DLS size distribution of DOPA-rGO (A) and DOX/DOPA-rGO (C). NIR absorption spectra of DOPA-rGO (B) and DOX/DOPA-rGO (D).

4.2. Formulation and characterization of the Thiol-Maleimide HA-Ch based hydrogels

After confirming the successful synthesis of HA-Thiol, dCh-Mal and DOX/DOPA-rGO, aqueous solutions containing these agents were prepared and mixed, leading to the assembly of the Thiol-Maleimide hydrogels incorporating this nanomaterial – termed as DOX/DOPA-rGO@TMgel (Figure 8). The same procedure was also applied using

DOPA-rGO, leading to the assembly of DOPA-rGO@TMgel. After this mixing process, the gelation of the hydrogels was confirmed by the inverted microtube test (Figure 18).

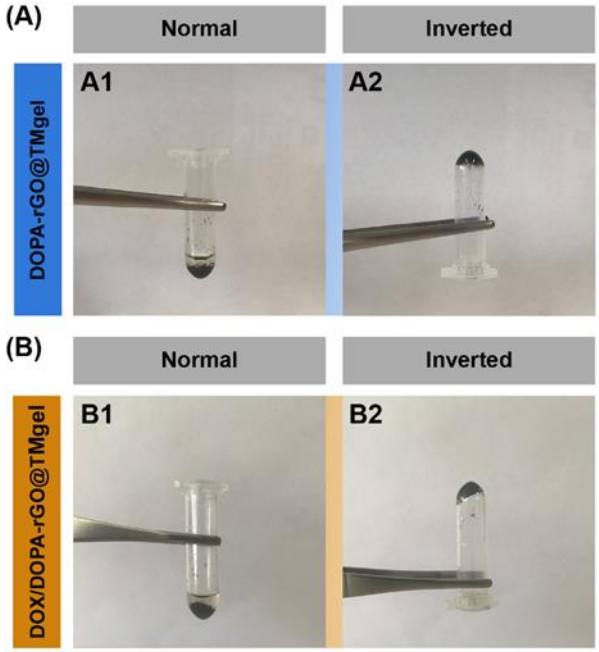

Figure 18: Macroscopic images of the gelation of the DOPA-rGO@TMgel (A1-2) and DOX/DOPA-rGO@TMgel (B1-2) assessed by the inverted microtube test.

As control, formulations without Maleimide groups (*i.e.,* prepared using dCh, HA-Thiol and DOPA-rGO) and without Thiol groups (*i.e.,* prepared using dCh-Mal, HA and DOPA-rGO) were also prepared – Figure 19. The formulations without Maleimide groups remained as solution and did not achieve gelation (Figure 19A1-2). The formulation prepared without Thiol groups appeared to precipitate, but no gelation was observed (Figure 19B1-2). Together, these results corroborate that the Thiol-Maleimide Michael type addition reaction between the HA-Thiol and dCh-Mal is crucial for the assembly of the DOPA-rGO@TMgel and DOX/DOPA-rGO@TMgel.

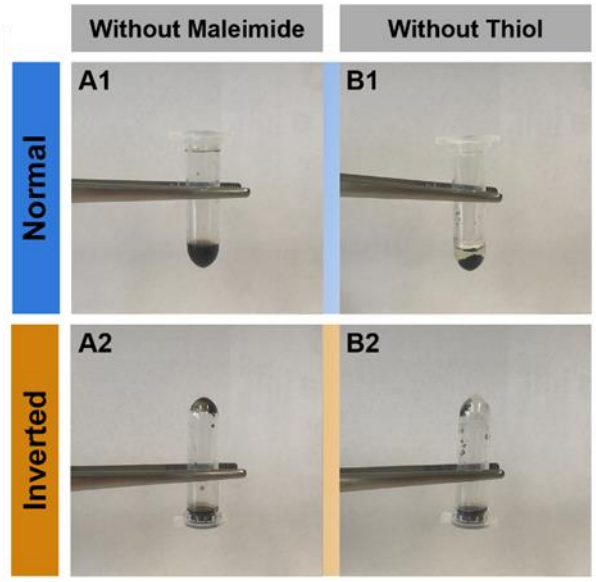

Figure 19: Macroscopic images of the inverted microtube test of the formulations prepared without Maleimide groups (*i.e.,* prepared using dCh, HA-Thiol and DOPA-rGO) (A1-A2) and without Thiol groups (*i.e.,* prepared using dCh-Mal, HA and DOPA-rGO) (B1-B2).

Subsequently, the morphology and porosity of the produced hydrogels was assessed by imaging their surface and interior (cross-section) by SEM (Figure 20). The DOPA-rGO@TMgel and DOX/DOPA-rGO@TMgel displayed a uniform porous structure at their surface (Figure 20A1 and 20B1) and interior (Figure 20A2 and 20B2), which is crucial for nanomaterials' diffusion (110). Moreover, the formulations' pores appeared to be highly interconnected, which is a characteristic of densely packed hydrogels such as those that are chemically crosslinked (111, 112).

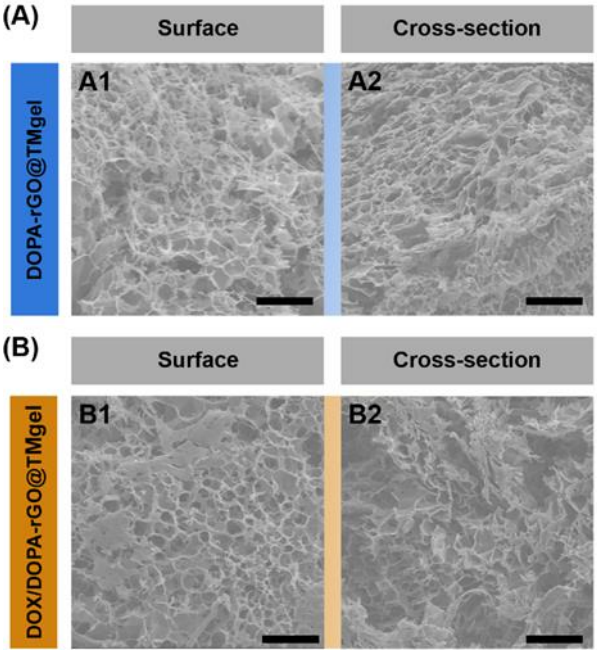

Figure 20: SEM images of the surface and cross-section of DOPA-rGO@TMgel (A1-2) and DOX/DOPA-rGO@TMgel (B1-2). Scale bars represent 100 μm.

Furthermore, the degradability of DOPA-rGO@TMgel and DOX/DOPA-rGO@TMgel, under conditions similar to the human physiological environment, was visualized by SEM (Figure 21). The images revealed an incubation-time dependent degradation of the polymeric network, both on the hydrogels' surface (Figure 21A-C) and interior (Figure 21D-F). This behavior is in line with the excellent biodegradability of Ch- and HA-based hydrogels (113-116). As importantly, it could be fundamental to allow the diffusion of the entrapped agents as well as eliminate the need to remove the hydrogels (by surgery) after their therapeutic effect (117, 118).

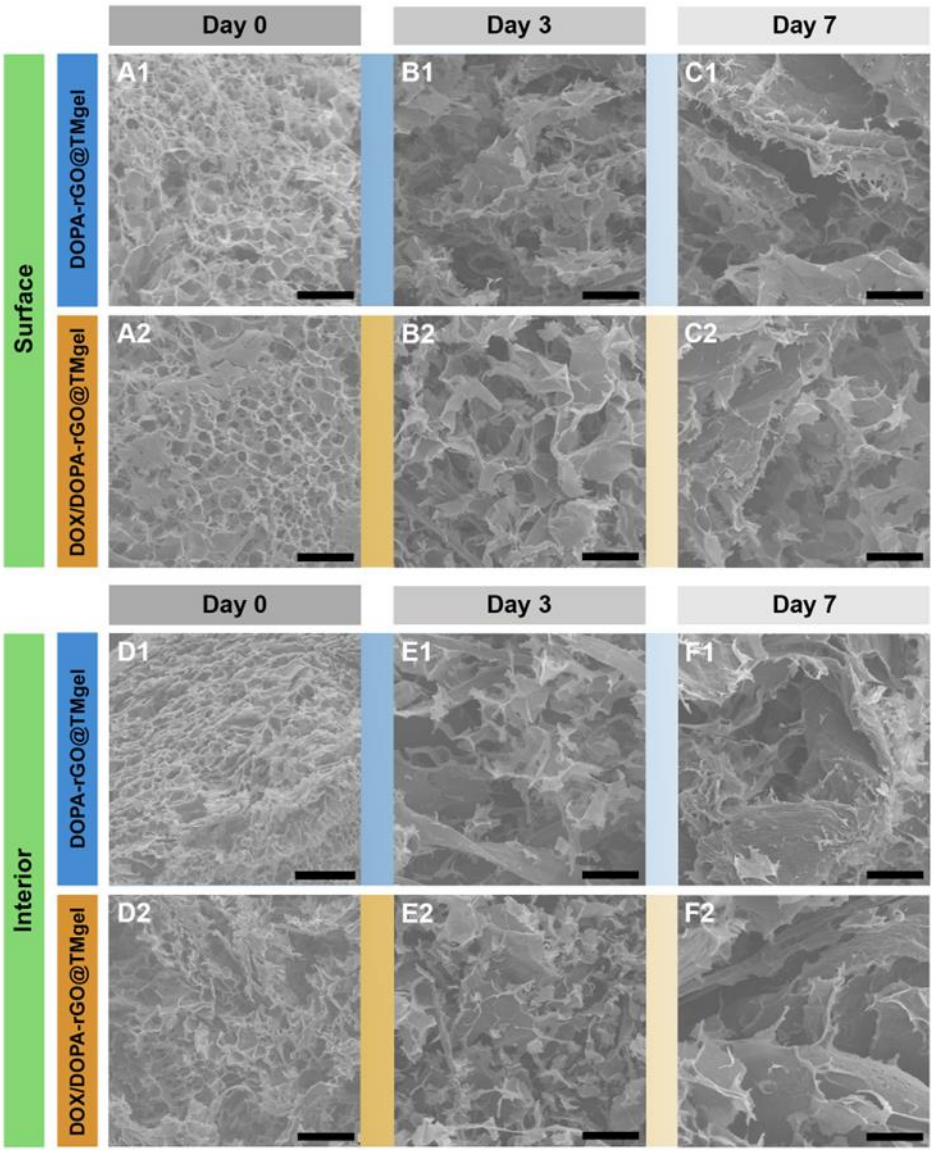

Figure 21: SEM images of DOPA-rGO@TMgel and DOX/DOPA-rGO@TMgel surface after 0 (A1, A2), 3 (B1, B2) and 7 (C1, C2) days of incubation in PBS (pH 7.4) supplemented with Lysozyme. SEM images of DOPA-rGO@TMgel and DOX/DOPA-rGO@TMgel interior (cross-section) after 0 (D1, D2), 3 (E1, E2) and 7 (F1, F2) days of incubation in the same conditions. Scale bar indicates 100 μm.

Afterwards, the long-term stability of the hydrogel precursor solutions was investigated (Figure 22 and 23). For this purpose, the aqueous solutions containing the individual polymers (HA-Thiol and dCh-Mal) and the therapeutic agents (DOPA-rGO or DOX/DOPA-rGO) were stored at 4 °C for a total of 7 days. As it can be seen in Figure 22, both DOPA-rGO and DOX/DOPA-rGO maintained their size distribution (Figure 22A and 22C) and NIR absorbance (Figure 22B and 22D). Such is crucial to ensure that these nanomaterials retain their therapeutic potential (related to their size and photothermal capacity) even after prolonged storage.

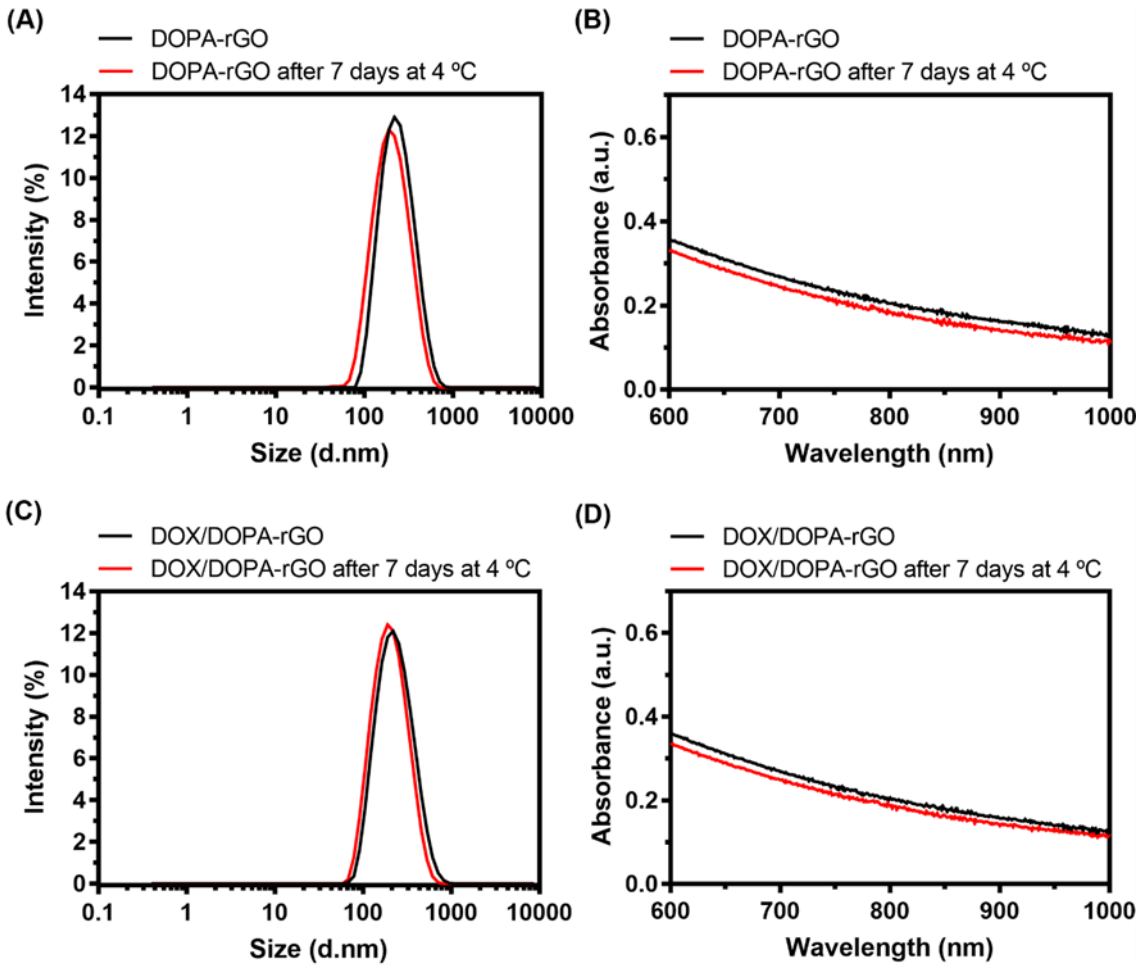

Figure 22: DLS size distribution (A) and NIR absorption (B) of as-prepared DOPA-rGO and after storage for 7 days at 4 °C. DLS size distribution (C) and NIR absorption (D) of as-prepared DOX/DOPA-rGO and after storage for 7 days at 4 °C.

As importantly, when all the aged/stored solutions were mixed, the DOPA-rGO@TMgel and DOX/DOPA-rGO@TMgel gelified in a similar manner (Figure 23), indicating that their ability to form Thiol-Maleimide bonds is retained.

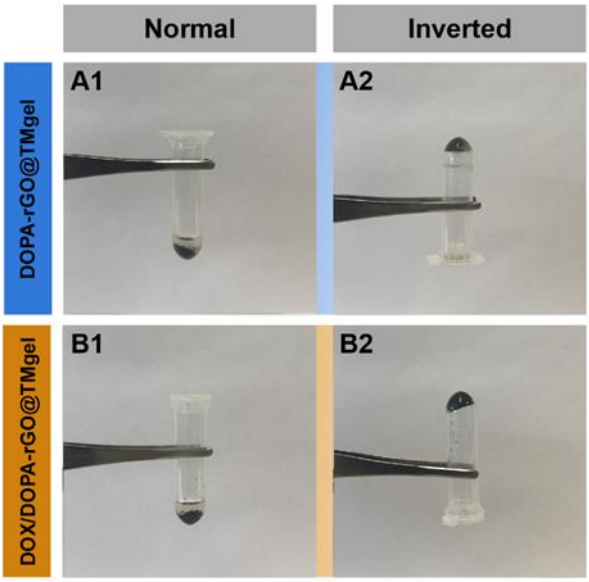

Figure 23: Inversion microtube test of DOPA-rGO@TMgel (A1-2) and DOX/DOPA-rGO@TMgel (B1-2) after storage of its precursor solutions for 7 days at 4 °C.

Then, the photothermal capacity of DOPA-rGO@TMgel and DOX/DOPA-rGO@TMgel was studied by irradiating them with NIR light (808 nm, 1.7 W/cm²) for 10 min, and measuring the attained temperature variations (ΔT) – Figure 24. As expected, the photoinduced heat generated by both formulations was dependent on the irradiation time (Figure 24). After 10 min of NIR laser exposure, both DOPA-rGO@TMgel and DOX/DOPA-rGO@TMgel produced a similar temperature increase of 21 – 22 °C, which can be explored to induce damage on cancer cells (119). A control test where water was exposed to NIR light showed a minimal temperature increase, which is in line with the low interaction of water with this radiation (120).

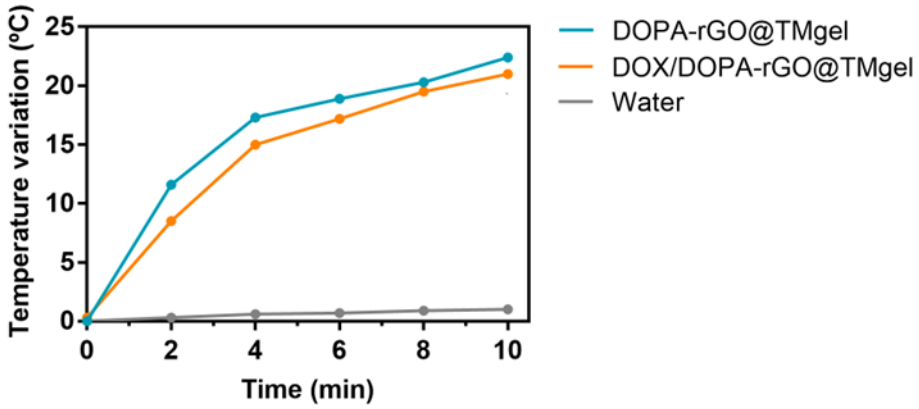

Figure 24: Temperature variation curves of DOPA-rGO@TMgel, DOX/DOPA-rGO@TMgel and water upon irradiation with NIR light (808 nm, 1.7 W/cm²) during 10 min.

In a recent work, Wu *et al.* created a methylcellulose-based hydrogel incorporating IR820 (500 µg/mL), which mediated a temperature increase of about 29 °C upon NIR irradiation (808 nm, 2 W/cm², 5 min) (121). Melo *et. al.* produced a Ch-$NaHCO_3$ based hydrogel that also contained DOPA-rGO (66.7 µg/mL), which produced a photoinduced heat of about 12 °C (808 nm, 1.7 W/cm², 10 min) (122). Herein, the DOPA-rGO@TMgel and DOX/DOPA-rGO@TMgel (150 µg/mL of DOPA-rGO) could generate a temperature increase of about 21 – 22 °C upon NIR laser exposure (808 nm, 1.7 W/cm², 10 min), demonstrating their good photothermal potential.

4.3. *In vitro* evaluation of the cytocompatibility of the DOPA-rGO@TMgel

After confirming the photothermal capacity of the hydrogels, the cytocompatibility profile of DOPA-rGO@TMgel in healthy (NHDF) and breast cancer (MCF-7) cells was assessed (Figure 25). Even after 48 h of incubation with this formulation, NHDF and MCF-7 cells remained with a viability of 70 % and 90 %, respectively. The good cytocompatibility of DOPA-rGO@TMgel may be related to the use of biocompatible polymers (HA and Ch) in its composition, as well as correlated with the good biological properties of DOPA-rGO (55, 123, 124). Lima-Sousa *et al.* developed a Ch and Agarose based hydrogel that incorporated rGO (reduced using Vitamin C), that also revealed a good cytocompatibility profile (98). Other Ch and HA-based hydrogels reported in the literature also displayed good biological properties (122, 125, 126). Taken together, these results also indicate that the Thiol and Maleimide modifications were not detrimental for the hydrogels' biological properties, highlighting the hydrogels' suitability for cancer therapy.

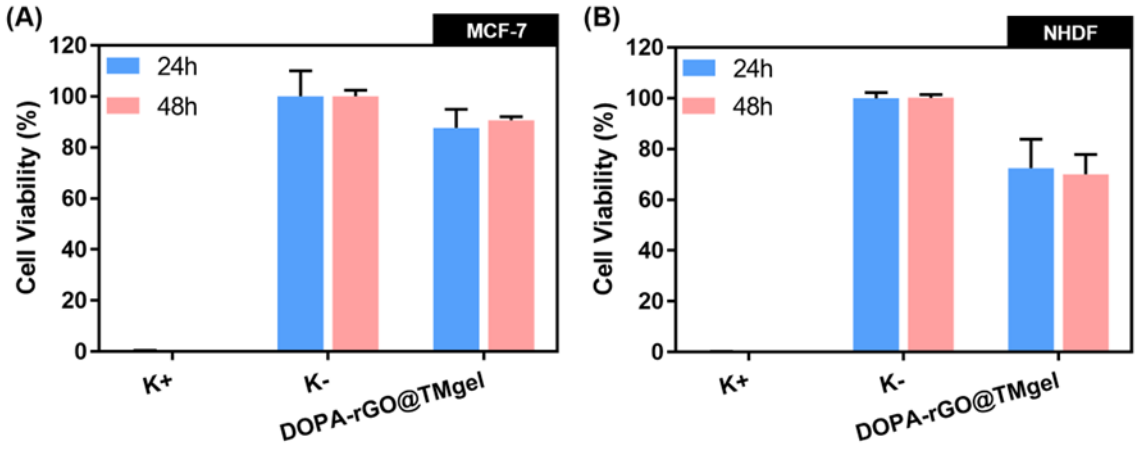

Figure 25: Cell viability of MCF-7 (A) and NHDF (B) after 24 and 48 h of incubation with DOPA-rGO@TMgel. Data represents mean ± S.D., n = 5. K^- represents the negative control and K^+ represents the positive control.

4.4. *In vitro* evaluation of the PTT mediated by DOPA-rGO@TMgel and chemo-PTT mediated by DOX/DOPA-rGO@TMgel

By last, the phototherapeutic and chemo-phototherapeutic effects mediated by DOPA-rGO@TMgel and DOX/DOPA-rGO@TMgel, respectively, were assessed on MCF-7 cells. For this assay, the formulations were incubated with the breast cancer cells and then irradiated with NIR light for 10 min (808 nm, 1.7 W/cm²) – Figure 26A.

As expected, the single use of NIR irradiation did not affect MCF-7 cells' viability (≈ 99 %), which is in line with the scarce temperature variation that is attained when water is exposed to NIR light (Figure 26B and Figure 24). On the other hand, when DOPA-rGO@TMgel was combined with NIR light (hydrogels' PTT), the breast cancer cells' viability showed a moderate decrease to 59 %. Closely, DOX/DOPA-rGO@TMgel (hydrogels' chemotherapy) only reduced the cells' viability to about 50 %. Interestingly, the combined action of DOX/DOPA-rGO@TMgel and NIR light (hydrogels' chemo-PTT) was able to reduce the breast cancer cells' viability to just 21 %.

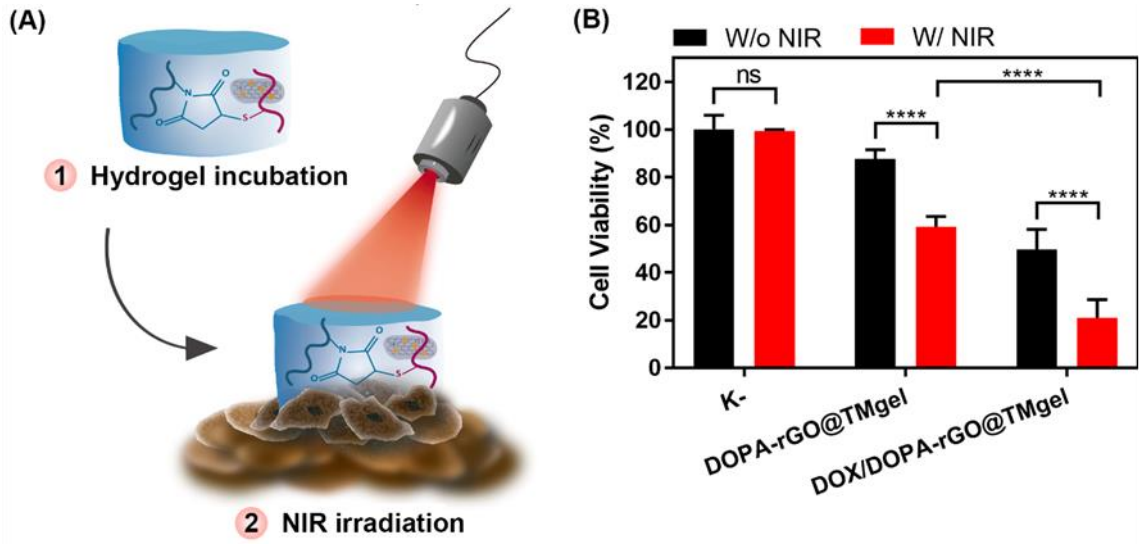

Figure 26: Schematic depicting the chemo-PTT mediated by DOX/DOPA-rGO@TMgel (A). Therapeutic effect of DOPA-rGO@TMgel (150 μg/mL of DOPA-rGO) and DOX/DOPA-rGO@TMgel (0.444 μg/mL of DOX; 150 μg/mL of DOPA-rGO) towards MCF-7 cells without (W/o NIR) and with (W/ NIR) NIR laser irradiation (808 nm, 1.7 W/cm², 10 min) (B). Data represents mean ± S.D., n = 5, $^{****}p < 0.0001$, ns = non-significant. K^- W/o NIR represents the negative control and K^- W/ NIR represents cells solely exposed to NIR light.

To confirm these results, breast cancer cells were also stained with Calcein-AM (labels live cells) and PI (labels dead cells) and imaged by CLSM (Figure 27). In concomitance with the cell viability results, cells exposed to just NIR light only displayed Calcein-AM fluorescence signals. In turn, the breast cancer cell populations exposed to

DOPA-rGO@TMgel plus NIR light (hydrogels' PTT) and DOX/DOPA-rGO@TMgel (hydrogels' chemotherapy) presented both Calcein-AM and PI fluorescence signals, indicating that these cells are only partially eliminated. In stark contrast, the majority of the breast cancer cells incubated with DOX/DOPA-rGO@TMgel plus NIR light revealed PI fluorescence signals, further confirming the enhanced therapeutic outcome arising from the hydrogels' chemo-PTT.

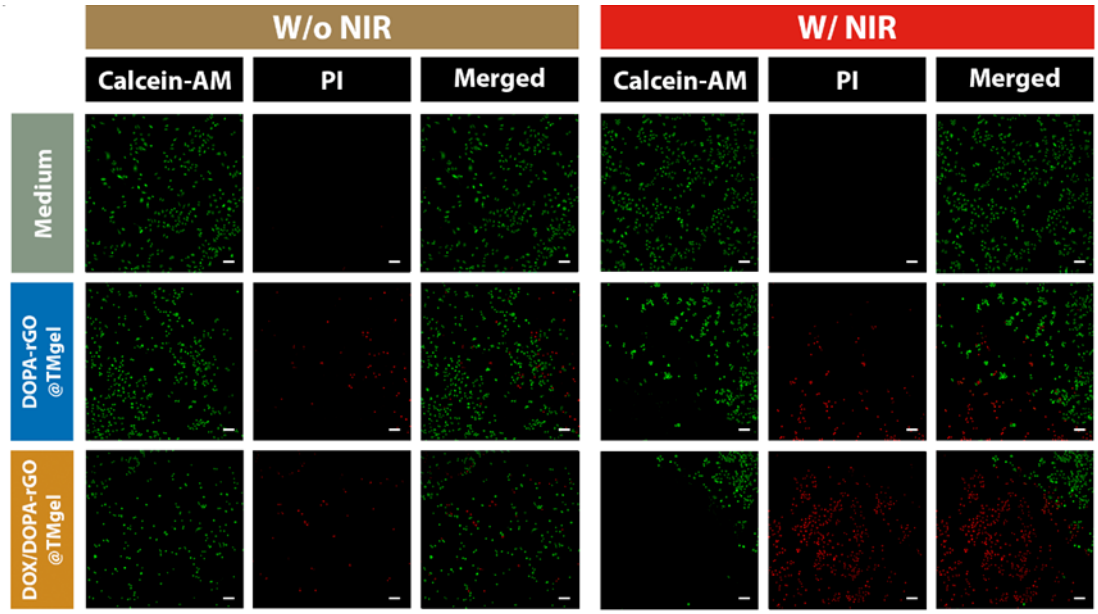

Figure 27: CLSM images of MCF-7 cells stained with Calcein-AM/PI after incubation with DOPA-rGO@TMgel (150 μg/mL of DOPA-rGO) or DOX/DOPA-rGO@TMgel (0.444 μg/mL of DOX; 150 μg/mL of DOPA-rGO) W/o NIR or W/ NIR laser irradiation (808 nm, 1.7 W/cm², 10 min). Medium W/o NIR represents the control for live cells, while Medium W/ NIR represents cells only exposed to NIR light. Green channel: Calcein-AM; red channel: PI. Scale bars correspond to 100 μm.

He *et al.* prepared a polypeptide based hydrogel containing black phosphorus nanosheets (400 μg/mL; photothermal agent) and Bufalin (50 nmol/L; chemotherapeutic agent) that, upon NIR irradiation (808 nm, 1.0 W/cm², 10 min), could decrease colon cancer cells' viability to about 27 % (127). In another work, Melo *et al.* produced an Ch-$NaHCO_3$ based hydrogel that incorporated DOPA-rGO (66.7 μg/mL) and Resveratrol (35 μg/mL), which upon NIR laser exposure (808 nm, 1.7 W/cm², 10 min), diminished the viability of breast cancer cells to about 31 % (122). Herein, the DOX/DOPA-rGO@TMgel (0.444 μg/mL of DOX; 150 μg/mL of DOPA-rGO) combined with NIR light (808 nm, 1.7 W/cm², 10 min) reduced the breast cancer cells' viability to just 21 %, highlighting its potential for chemo-PTT.

Chapter 5

Conclusion and Future Perspectives

5. Conclusion and Future Perspectives

Despite the huge scientific advances, breast cancer still persists as a deadly disease. In fact, the currently employed therapies for this type of cancer (*e.g.* surgery, chemotherapy, radiotherapy) have several limitations, being highly inefficient, which is reflected by a high mortality rate. Moreover, these therapies are also highly invasive and bring significant side effects. In this way, effective approaches with an improved specificity are still in demand for breast cancer.

Scientists have been exploring the potential of nanomaterials for cancer therapy. In this regard, NIR light responsive nanomaterials are of particular interest. These nanostructures, after accumulation at the tumor site and interaction with NIR light, can cause cellular damage through hyperthermia (PTT). Furthermore, the core of these nanomaterials can also be loaded with chemotherapeutic drugs, paving the way for a localized synergistic combinatorial therapy. Notwithstanding, the discouraging reality is that less than 1 % of the systemically administered nano-formulations reach the tumor zone.

To overcome the poor-tumor homing capacity of systemically administered nanomaterials, their local delivery using Thiol-Maleimide Michael type addition hydrogels is a promising approach. This macro-scale system presents ability to incorporate high doses of nanoparticles into their compact 3D structure as well as good chemical selectivity, biocompatibility, and simple construction. However, such hydrogels have been mostly prepared using synthetic polymers, which is not ideal considering their non-biodegradability.

Herein, a novel Thiol-Maleimide crosslinked hydrogel, based on natural polymers, was produced for application in the chemo-PTT of breast cancer cells. For obtaining natural polymers compatible with this crosslinking chemistry, HA was decorated with Cysteine and dCh was grafted with Sulfo-SMCC. Simultaneously, DOPA-rGO was produced and loaded with DOX to create NIR light responsive nanomaterial with chemo-PTT capabilities. By simply mixing HA-Thiol, dCh-Mal, and DOX/DOPA-rGO, Thiol-Maleimide crosslinked hydrogels incorporating this chemo-photothermal nanomaterial could be assembled (DOX/DOPA-rGO@TMgel). For comparative purposes, DOPA-rGO@TMgel was also assembled using the above-described polymers and DOPA-rGO.

Both DOPA-rGO@TMgel and DOX/DOPA-rGO@TMgel presented a suitable gelation as well as a good porosity. Upon interaction with NIR radiation, these hydrogels could produce a temperature increase of approximately 22 °C, revealing a good photothermal capacity. In *in vitro* studies, the DOPA-rGO@TMgel revealed a good cytocompatibility towards both healthy and breast cancer cells. When breast cancer cells were incubated with DOPA-rGO@TMgel and exposed to NIR light (hydrogels' PTT), their viability was reduced to about 59 %. On the other hand, DOX/DOPA-rGO@TMgel (hydrogels' chemotherapy) diminished cancer cells' viability to 50 %. In stark contrast, the combined action of DOX/DOPA-rGO@TMgel and NIR light decreased breast cancer cells' viability to just 21 %, highlighting its chemo-phototherapeutic potential.

In the future, it will be important to investigate the behavior of chemo-PTT mediated by DOX/DOPA-rGO@TMgel in spheroids. This 3D *in vitro* tumor model replicates the key features of solid tumors, including cancer cell behavior, 3D morphology, and physical and biochemical barriers/resistance patterns (128, 129). Thereby, the use of spheroids in the screening of DOX/DOPA-rGO@TMgel efficacy will allow a closer estimation of its *in vivo* potential (128, 129). Still, *in vivo* studies will be crucial to analyze the long-term biocompatibility of this formulation as well as its applicability on postoperative chemo-PTT. On the other hand, different classes of therapeutic agents (*e.g*. Toll-like Receptor agonists, Immune checkpoint inhibitors) could also be incorporated in this hydrogel formulation in order to reach an even greater therapeutic outcome. Overall, the development of hydrogels for the tumor-confined delivery of anticancer agents can contribute to more effective and selective therapies, and thus, in the future, may assist in the reduction of cancer mortality.

Chapter 6

Bibliographic References

6. Bibliographic References

1. Sung H, Ferlay J, Siegel RL, Laversanne M, Soerjomataram I, Jemal A, et al. Global Cancer Statistics 2020: GLOBOCAN Estimates of Incidence and Mortality Worldwide for 36 Cancers in 185 Countries. CA: A Cancer Journal for Clinicians. 2021;71(3):209-49.
2. Hassanpour SH, Dehghani M. Review of cancer from perspective of molecular. Journal of Cancer Research and Practice. 2017;4(4):127-9.
3. Siegel RL, Miller KD, Fuchs HE, Jemal A. Cancer statistics, 2022. CA: A Cancer Journal for Clinicians. 2022;72(1):7-33.
4. Um P. Cancer, Definition. In: Highlander SK, Rodriguez-Valera F, White BA, editors. Encyclopedia of Metagenomics: Environmental Metagenomics. Boston, MA: Springer US; 2015. p. 65-.
5. Van Roosbroeck K, Calin GA. Chapter Four - Cancer Hallmarks and MicroRNAs: The Therapeutic Connection. In: Croce CM, Fisher PB, editors. Advances in Cancer Research. 135: Academic Press; 2017. p. 119-49.
6. Lippi G, Mattiuzzi C, Cervellin G. Meat consumption and cancer risk: a critical review of published meta-analyses. Critical Reviews in Oncology/Hematology. 2016;97:1-14.
7. Willenbrink TJ, Ruiz ES, Cornejo CM, Schmults CD, Arron ST, Jambusaria-Pahlajani A. Field cancerization: Definition, epidemiology, risk factors, and outcomes. Journal of the American Academy of Dermatology. 2020;83(3):709-17.
8. Whiteman DC, Wilson LF. The fractions of cancer attributable to modifiable factors: A global review. Cancer Epidemiology. 2016;44:203-21.
9. Senga SS, Grose RP. Hallmarks of cancer—the new testament. Open Biology. 2021;11(1):200358.
10. Darwiche N. Epigenetic mechanisms and the hallmarks of cancer: an intimate affair. Am J Cancer Res. 2020;10(7):1954-78.
11. Hanahan D, Weinberg Robert A. Hallmarks of Cancer: The Next Generation. Cell. 2011;144(5):646-74.
12. Hanahan D. Hallmarks of Cancer: New Dimensions. Cancer Discov. 2022;12(1):31-46.
13. Fouad YA, Aanei C. Revisiting the hallmarks of cancer. Am J Cancer Res. 2017;7(5):1016-36.
14. Oh DY, Fong L. Cytotoxic CD4+ T cells in cancer: Expanding the immune effector toolbox. Immunity. 2021;54(12):2701-11.
15. Pickup MW, Mouw JK, Weaver VM. The extracellular matrix modulates the hallmarks of cancer. EMBO Rep. 2014;15(12):1243-53.

16. Feng Y, Spezia M, Huang S, Yuan C, Zeng Z, Zhang L, et al. Breast cancer development and progression: Risk factors, cancer stem cells, signaling pathways, genomics, and molecular pathogenesis. Genes Dis. 2018;5(2):77-106.
17. Place AE, Jin Huh S, Polyak K. The microenvironment in breast cancer progression: biology and implications for treatment. Breast Cancer Research. 2011;13(6):227.
18. Soysal SD, Tzankov A, Muenst SE. Role of the Tumor Microenvironment in Breast Cancer. Pathobiology. 2015;82(3-4):142-52.
19. McGuire KP. Breast Anatomy and Physiology. In: Aydiner A, Igci A, Soran A, editors. Breast Disease: Diagnosis and Pathology, Volume 1. Cham: Springer International Publishing; 2019. p. 1-9.
20. Sun Y-S, Zhao Z, Yang Z-N, Xu F, Lu H-J, Zhu Z-Y, et al. Risk Factors and Preventions of Breast Cancer. International Journal of Biological Sciences. 2017;13(11):1387-97.
21. Libson S, Lippman M. A review of clinical aspects of breast cancer. International Review of Psychiatry. 2014;26(1):4-15.
22. Veronesi U, Boyle P, Goldhirsch A, Orecchia R, Viale G. Breast cancer. Lancet. 2005;365(9472):1727-41.
23. Simon A, Robb K. Cancer: breast. In: Baum A, McManus C, Weinman J, Wallston K, West R, Newman S, et al., editors. Cambridge Handbook of Psychology, Health and Medicine. 2 ed. Cambridge: Cambridge University Press; 2007. p. 577-80.
24. Burstein HJ, Polyak K, Wong JS, Lester SC, Kaelin CM. Ductal Carcinoma in Situ of the Breast. New England Journal of Medicine. 2004;350(14):1430-41.
25. Polyak K. Breast cancer: origins and evolution. Journal of Clinical Investigation. 2007;117(11):3155-63.
26. Boix-Montesinos P, Soriano-Teruel PM, Armiñán A, Orzáez M, Vicent MJ. The past, present, and future of breast cancer models for nanomedicine development. Advanced Drug Delivery Reviews. 2021;173:306-30.
27. Radecka B, Litwiniuk M. Breast cancer in young women. Ginekologia Polska. 2016;87(9):659-63.
28. McDonald ES, Clark AS, Tchou J, Zhang P, Freedman GM. Clinical Diagnosis and Management of Breast Cancer. Journal of Nuclear Medicine. 2016;57(Supplement 1):9S-16S.
29. Moo T-A, Sanford R, Dang C, Morrow M. Overview of Breast Cancer Therapy. PET Clinics. 2018;13(3):339-54.

30. Pais-Silva C, de Melo-Diogo D, Correia IJ. IR780-loaded TPGS-TOS micelles for breast cancer photodynamic therapy. European Journal of Pharmaceutics and Biopharmaceutics. 2017;113:108-17.
31. Bazak R, Houri M, Achy SE, Hussein W, Refaat T. Passive targeting of nanoparticles to cancer: A comprehensive review of the literature. Molecular and Clinical Oncology. 2014;2(6):904-8.
32. Fernandes N, Rodrigues CF, Moreira AF, Correia IJ. Overview of the application of inorganic nanomaterials in cancer photothermal therapy. Biomaterials Science. 2020;8(11):2990-3020.
33. Yao Y, Zhou Y, Liu L, Xu Y, Chen Q, Wang Y, et al. Nanoparticle-Based Drug Delivery in Cancer Therapy and Its Role in Overcoming Drug Resistance. Front Mol Biosci. 2020;7:193.
34. Kumar AVP, Dubey SK, Tiwari S, Puri A, Hejmady S, Gorain B, et al. Recent advances in nanoparticles mediated photothermal therapy induced tumor regression. Int J Pharm. 2021;606:120848.
35. Li Y, Zhang H. Nanoparticle-Based Drug Delivery Systems for Enhanced Tumor-Targeting Treatment. J Biomed Nanotechnol. 2019;15(1):1-27.
36. Torchilin V. Tumor delivery of macromolecular drugs based on the EPR effect. Adv Drug Deliv Rev. 2011;63(3):131-5.
37. Markman JL, Rekechenetskiy A, Holler E, Ljubimova JY. Nanomedicine therapeutic approaches to overcome cancer drug resistance. Adv Drug Deliv Rev. 2013;65(13-14):1866-79.
38. Rodrigues CF, Alves CG, Lima-Sousa R, Moreira AF, de Melo-Diogo D, Correia IJ. Chapter 10 - Inorganic-based drug delivery systems for cancer therapy. In: Singh MR, Singh D, Kanwar JR, Chauhan NS, editors. Advances and Avenues in the Development of Novel Carriers for Bioactives and Biological Agents: Academic Press; 2020. p. 283-316.
39. Nie S. Understanding and overcoming major barriers in cancer nanomedicine. Nanomedicine. 2010;5(4):523-8.
40. Luo Z, Dai Y, Gao H. Development and application of hyaluronic acid in tumor targeting drug delivery. Acta Pharm Sin B. 2019;9(6):1099-112.
41. Chaturvedi VK, Singh A, Singh VK, Singh MP. Cancer Nanotechnology: A New Revolution for Cancer Diagnosis and Therapy. Curr Drug Metab. 2019;20(6):416-29.
42. de Melo-Diogo D, Pais-Silva C, Dias DR, Moreira AF, Correia IJ. Strategies to Improve Cancer Photothermal Therapy Mediated by Nanomaterials. Advanced Healthcare Materials. 2017;6(10):1700073.

43. Han HS, Choi KY. Advances in Nanomaterial-Mediated Photothermal Cancer Therapies: Toward Clinical Applications. Biomedicines. 2021;9(3):305.
44. Chu KF, Dupuy DE. Thermal ablation of tumours: biological mechanisms and advances in therapy. Nature Reviews Cancer. 2014;14(3):199-208.
45. Pizzino G, Irrera N, Cucinotta M, Pallio G, Mannino F, Arcoraci V, et al. Oxidative Stress: Harms and Benefits for Human Health. Oxidative Medicine and Cellular Longevity. 2017;2017:1-13.
46. Nikfarjam M, Muralidharan V, Christophi C. Mechanisms of focal heat destruction of liver tumors. J Surg Res. 2005;127(2):208-23.
47. Yang W, Liang H, Ma S, Wang D, Huang J. Gold nanoparticle based photothermal therapy: Development and application for effective cancer treatment. Sustainable Materials and Technologies. 2019;22:e00109.
48. Li X, Lovell JF, Yoon J, Chen X. Clinical development and potential of photothermal and photodynamic therapies for cancer. Nature Reviews Clinical Oncology. 2020;17(11):657-74.
49. Jung HS, Verwilst P, Sharma A, Shin J, Sessler JL, Kim JS. Organic molecule-based photothermal agents: an expanding photothermal therapy universe. Chemical Society Reviews. 2018;47(7):2280-97.
50. Liu L, Ma Q, Cao J, Gao Y, Han S, Liang Y, et al. Recent progress of graphene oxide-based multifunctional nanomaterials for cancer treatment. Cancer Nanotechnology. 2021;12(1).
51. Lima-Sousa R, de Melo-Diogo D, Alves CG, Costa EC, Ferreira P, Louro RO, et al. Hyaluronic acid functionalized green reduced graphene oxide for targeted cancer photothermal therapy. Carbohydrate Polymers. 2018;200:93-9.
52. Dash BS, Jose G, Lu Y-J, Chen J-P. Functionalized Reduced Graphene Oxide as a Versatile Tool for Cancer Therapy. International Journal of Molecular Sciences. 2021;22(6):2989.
53. Taniselass S, Md Arshad MK, Gopinath SCB. Current state of green reduction strategies: Solution-processed reduced graphene oxide for healthcare biodetection. Materials Science and Engineering: C. 2019;96:904-14.
54. Thakur S, Karak N. Alternative methods and nature-based reagents for the reduction of graphene oxide: A review. Carbon. 2015;94:224-42.
55. Lima-Sousa R, Alves CG, Melo BL, Moreira AF, Mendonça AG, Correia IJ, et al. Poly(2-ethyl-2-oxazoline) functionalized reduced graphene oxide: Optimization of the reduction process using dopamine and application in cancer photothermal therapy. Materials Science and Engineering: C. 2021;130:112468.

56. Mó I, Alves CG, De Melo-Diogo D, Lima-Sousa R, Correia IJ. Assessing the Combinatorial Chemo-Photothermal Therapy Mediated by Sulfobetaine Methacrylate-Functionalized Nanoparticles in 2D and 3D In Vitro Cancer Models. Biotechnology Journal. 2020;15(12):2000219.
57. Jin A, Wang Y, Lin K, Jiang L. Nanoparticles modified by polydopamine: Working as "drug" carriers. Bioact Mater. 2020;5(3):522-41.
58. Wang Z, Duan Y, Duan Y. Application of polydopamine in tumor targeted drug delivery system and its drug release behavior. Journal of Controlled Release. 2018;290:56-74.
59. Motlagh NSH, Parvin P, Mirzaie ZH, Karimi R, Sanderson JH, Atyabi F. Synergistic performance of triggered drug release and photothermal therapy of MCF7 cells based on laser activated PEGylated GO + DOX. Biomed Opt Express. 2020;11(7):3783-94.
60. Wilhelm S, Tavares AJ, Dai Q, Ohta S, Audet J, Dvorak HF, et al. Analysis of nanoparticle delivery to tumours. Nature Reviews Materials. 2016;1(5):16014.
61. Blanco E, Shen H, Ferrari M. Principles of nanoparticle design for overcoming biological barriers to drug delivery. Nature Biotechnology. 2015;33(9):941-51.
62. Thomas OS, Weber W. Overcoming Physiological Barriers to Nanoparticle Delivery-Are We There Yet? Front Bioeng Biotechnol. 2019;7:415.
63. Suk JS, Xu Q, Kim N, Hanes J, Ensign LM. PEGylation as a strategy for improving nanoparticle-based drug and gene delivery. Advanced Drug Delivery Reviews. 2016;99:28-51.
64. Sanchez L, Yi Y, Yu Y. Effect of partial PEGylation on particle uptake by macrophages. Nanoscale. 2017;9(1):288-97.
65. Owens DE, Peppas NA. Opsonization, biodistribution, and pharmacokinetics of polymeric nanoparticles. International Journal of Pharmaceutics. 2006;307(1):93-102.
66. Matsumoto Y, Nichols JW, Toh K, Nomoto T, Cabral H, Miura Y, et al. Vascular bursts enhance permeability of tumour blood vessels and improve nanoparticle delivery. Nature Nanotechnology. 2016;11(6):533-8.
67. Sindhwani S, Syed AM, Ngai J, Kingston BR, Maiorino L, Rothschild J, et al. The entry of nanoparticles into solid tumours. Nature Materials. 2020;19(5):566-75.
68. Zhao Z, Ukidve A, Kim J, Mitragotri S. Targeting Strategies for Tissue-Specific Drug Delivery. Cell. 2020;181(1):151-67.
69. Moreira AF, Rodrigues CF, Jacinto TA, Miguel SP, Costa EC, Correia IJ. Microneedle-based delivery devices for cancer therapy: A review. Pharmacological Research. 2019;148:104438.

70. Kearney CJ, Mooney DJ. Macroscale delivery systems for molecular and cellular payloads. Nature Materials. 2013;12(11):1004-17.
71. Sun Z, Song C, Wang C, Hu Y, Wu J. Hydrogel-Based Controlled Drug Delivery for Cancer Treatment: A Review. Molecular Pharmaceutics. 2020;17(2):373-91.
72. Batista RA, Otoni CG, Espitia PJP. Chapter 3 - Fundamentals of chitosan-based hydrogels: elaboration and characterization techniques. In: Holban A-M, Grumezescu AM, editors. Materials for Biomedical Engineering: Elsevier; 2019. p. 61-81.
73. Dimatteo R, Darling NJ, Segura T. In situ forming injectable hydrogels for drug delivery and wound repair. Adv Drug Deliv Rev. 2018;127:167-84.
74. Parhi R. Cross-Linked Hydrogel for Pharmaceutical Applications: A Review. Adv Pharm Bull. 2017;7(4):515-30.
75. Hu W, Wang Z, Xiao Y, Zhang S, Wang J. Advances in crosslinking strategies of biomedical hydrogels. Biomaterials Science. 2019;7(3):843-55.
76. Xiao Y, Gu Y, Qin L, Chen L, Chen X, Cui W, et al. Injectable thermosensitive hydrogel-based drug delivery system for local cancer therapy. Colloids and Surfaces B: Biointerfaces. 2021;200:111581.
77. Chyzy A, Tomczykowa M, Plonska-Brzezinska ME. Hydrogels as Potential Nano-, Micro- and Macro-Scale Systems for Controlled Drug Delivery. Materials. 2020;13(1):188.
78. Shen H, Gao Q, Ye Q, Yang S, Wu Y, Huang Q, et al. Peritumoral implantation of hydrogel-containing nanoparticles and losartan for enhanced nanoparticle penetration and antitumor effect. International Journal of Nanomedicine. 2018;Volume 13:7409-26.
79. Ding D, Zhu Z, Li R, Li X, Wu W, Jiang X, et al. Nanospheres-Incorporated Implantable Hydrogel as a Trans-Tissue Drug Delivery System. ACS Nano. 2011;5(4):2520-34.
80. Li J, Mooney DJ. Designing hydrogels for controlled drug delivery. Nature Reviews Materials. 2016;1(12):16071.
81. Nair DP, Podgórski M, Chatani S, Gong T, Xi W, Fenoli CR, et al. The Thiol-Michael Addition Click Reaction: A Powerful and Widely Used Tool in Materials Chemistry. Chemistry of Materials. 2014;26(1):724-44.
82. Guaresti O, Basasoro S, González K, Eceiza A, Gabilondo N. In situ cross–linked chitosan hydrogels via Michael addition reaction based on water–soluble thiol–maleimide precursors. European Polymer Journal. 2019;119:376-84.
83. Yin C, Huo F, Zhang J, Martínez-Máñez R, Yang Y, Lv H, et al. Thiol-addition reactions and their applications in thiol recognition. Chemical Society Reviews. 2013;42(14):6032.

84. Mather BD, Viswanathan K, Miller KM, Long TE. Michael addition reactions in macromolecular design for emerging technologies. Progress in Polymer Science. 2006;31(5):487-531.
85. Gober IN, Riemen AJ, Villain M. Sequence sensitivity and pH dependence of maleimide conjugated N-terminal cysteine peptides to thiazine rearrangement. Journal of Peptide Science. 2021;27(7):e3323.
86. Ravasco JMJM, Faustino H, Trindade A, Gois PMP. Bioconjugation with Maleimides: A Useful Tool for Chemical Biology. Chemistry – A European Journal. 2019;25(1):43-59.
87. Patrulea V, Ostafe V, Borchard G, Jordan O. Chitosan as a starting material for wound healing applications. European Journal of Pharmaceutics and Biopharmaceutics. 2015;97:417-26.
88. Muxika A, Etxabide A, Uranga J, Guerrero P, de la Caba K. Chitosan as a bioactive polymer: Processing, properties and applications. Int J Biol Macromol. 2017;105(Pt 2):1358-68.
89. Matsumoto M, Udomsinprasert W, Laengee P, Honsawek S, Patarakul K, Chirachanchai S. A Water-Based Chitosan-Maleimide Precursor for Bioconjugation: An Example of a Rapid Pathway for an In Situ Injectable Adhesive Gel. Macromolecular Rapid Communications. 2016;37(19):1618-22.
90. El-Sayed NS, Shirazi AN, El-Meligy MG, El-Ziaty AK, Nagieb ZA, Parang K, et al. Design, synthesis, and evaluation of chitosan conjugated GGRGDSK peptides as a cancer cell-targeting molecular transporter. International Journal of Biological Macromolecules. 2016;87:611-22.
91. Neuman MG, Nanau RM, Oruña-Sanchez L, Coto G. Hyaluronic acid and wound healing. J Pharm Pharm Sci. 2015;18(1):53-60.
92. Jin R, Moreira Teixeira LS, Krouwels A, Dijkstra PJ, van Blitterswijk CA, Karperien M, et al. Synthesis and characterization of hyaluronic acid–poly(ethylene glycol) hydrogels via Michael addition: An injectable biomaterial for cartilage repair. Acta Biomaterialia. 2010;6(6):1968-77.
93. Xu X, Jha AK, Harrington DA, Farach-Carson MC, Jia X. Hyaluronic acid-based hydrogels: from a natural polysaccharide to complex networks. Soft Matter. 2012;8(12):3280.
94. Poole LB. The basics of thiols and cysteines in redox biology and chemistry. Free Radical Biology and Medicine. 2015;80:148-57.
95. Gaspar VM, Sousa F, Queiroz JA, Correia IJ. Formulation of chitosan–TPP–pDNA nanocapsules for gene therapy applications. Nanotechnology. 2010;22(1):015101.

96. Pereira de Sousa I, Suchaoin W, Zupančič O, Leichner C, Bernkop-Schnürch A. Totally S-protected hyaluronic acid: Evaluation of stability and mucoadhesive properties as liquid dosage form. Carbohydr Polym. 2016;152:632-8.
97. Melo BL, Lima-Sousa R, Alves CG, Ferreira P, Moreira AF, Correia IJ, et al. Sulfobetaine methacrylate-albumin-coated graphene oxide incorporating IR780 for enhanced breast cancer phototherapy. Nanomedicine. 2021;16(6):453-64.
98. Lima-Sousa R, de Melo-Diogo D, Alves CG, Cabral CSD, Miguel SP, Mendonça AG, et al. Injectable in situ forming thermo-responsive graphene based hydrogels for cancer chemo-photothermal therapy and NIR light-enhanced antibacterial applications. Mater Sci Eng C Mater Biol Appl. 2020;117:111294.
99. Sabino IJ, Lima-Sousa R, Alves CG, Melo BL, Moreira AF, Correia IJ, et al. Injectable in situ forming hydrogels incorporating dual-nanoparticles for chemo-photothermal therapy of breast cancer cells. Int J Pharm. 2021;600:120510.
100. Battampara P, Nimisha Sathish T, Reddy R, Guna V, Nagananda GS, Reddy N, et al. Properties of chitin and chitosan extracted from silkworm pupae and egg shells. Int J Biol Macromol. 2020;161:1296-304.
101. Geçer A, Yıldız N, Çalımlı A, Turan B. Trimethyl chitosan nanoparticles enhances dissolution of the poorly water soluble drug Candesartan-Cilexetil. Macromolecular Research. 2010;18(10):986-91.
102. Batista MKS, Pinto LF, Gomes CAR, Gomes P. Novel highly-soluble peptide–chitosan polymers: Chemical synthesis and spectral characterization. Carbohydrate Polymers. 2006;64(2):299-305.
103. Nie X, Zhang J, Xu Q, Liu X, Li Y, Wu Y, et al. Targeting peptide iRGD-conjugated amphiphilic chitosan-co-PLA/DPPE drug delivery system for enhanced tumor therapy. Journal of Materials Chemistry B. 2014;2(21):3232.
104. Sahatsapan N, Rojanarata T, Ngawhirunpat T, Opanasopit P, Tonglairoum P. 6-Maleimidohexanoic acid-grafted chitosan: A new generation mucoadhesive polymer. Carbohydrate Polymers. 2018;202:258-64.
105. Pan NC, Pereira HCB, Da Silva MDLC, Vasconcelos AFD, Celligoi MAPC. Improvement Production of Hyaluronic Acid by Streptococcus zooepidemicus in Sugarcane Molasses. Applied Biochemistry and Biotechnology. 2017;182(1):276-93.
106. Yegappan R, Selvaprithiviraj V, Mohandas A, Jayakumar R. Nano polydopamine crosslinked thiol-functionalized hyaluronic acid hydrogel for angiogenic drug delivery. Colloids and Surfaces B: Biointerfaces. 2019;177:41-9.
107. Dong L, Chen H, Liu T, Zhu J, Yu M, Yuan Q. Poly(l-cysteine) Peptide Amphiphile Derivatives Containing Disulfide Bonds: Synthesis, Self-Assembly-Induced β-Sheet

Nanostructures, pH/Reduction Dual Response, and Drug Release. Biomacromolecules. 2021;22(12):5374-81.
108. Wu J. The Enhanced Permeability and Retention (EPR) Effect: The Significance of the Concept and Methods to Enhance Its Application. Journal of Personalized Medicine. 2021;11(8):771.
109. Vankayala R, Hwang KC. Near-Infrared-Light-Activatable Nanomaterial-Mediated Phototheranostic Nanomedicines: An Emerging Paradigm for Cancer Treatment. Advanced Materials. 2018;30(23):1706320.
110. Ganguly S, Margel S. Design of Magnetic Hydrogels for Hyperthermia and Drug Delivery. Polymers. 2021;13(23):4259.
111. Liu Z, Fan L, Xiao H, Cao C. A multiple covalent crosslinked soft hydrogel for bioseparation. Chemical Communications. 2016;52(15):3247-50.
112. Xie R, Chen Y-C, Zhao Y, Yodsanit N, Wang Y, Yamamoto N, et al. Injectable Hydrogel Capable of In Situ Covalent Crosslinking for Permanent Embolization. ACS Applied Materials & Interfaces. 2021;13(48):56988-99.
113. Ahmadi F, Oveisi Z, Samani SM, Amoozgar Z. Chitosan based hydrogels: characteristics and pharmaceutical applications. Res Pharm Sci. 2015;10(1):1-16.
114. Shariatinia Z, Jalali AM. Chitosan-based hydrogels: Preparation, properties and applications. International Journal of Biological Macromolecules. 2018;115:194-220.
115. Trombino S, Servidio C, Curcio F, Cassano R. Strategies for Hyaluronic Acid-Based Hydrogel Design in Drug Delivery. Pharmaceutics. 2019;11(8):407.
116. Park SH, Seo JY, Park JY, Ji YB, Kim K, Choi HS, et al. An injectable, click-crosslinked, cytomodulin-modified hyaluronic acid hydrogel for cartilage tissue engineering. NPG Asia Materials. 2019;11(1).
117. Ozcelik B. 7 - Degradable hydrogel systems for biomedical applications. In: Poole-Warren L, Martens P, Green R, editors. Biosynthetic Polymers for Medical Applications: Woodhead Publishing; 2016. p. 173-88.
118. Sheth S, Barnard E, Hyatt B, Rathinam M, Zustiak SP. Predicting Drug Release From Degradable Hydrogels Using Fluorescence Correlation Spectroscopy and Mathematical Modeling. Front Bioeng Biotechnol. 2019;7:410.
119. Huang X, Jain PK, El-Sayed IH, El-Sayed MA. Determination of the Minimum Temperature Required for Selective Photothermal Destruction of Cancer Cells with the Use of Immunotargeted Gold Nanoparticles. Photochemistry and Photobiology. 2006;82(2):412.
120. Shanmugam V, Selvakumar S, Yeh C-S. Near-infrared light-responsive nanomaterials in cancer therapeutics. Chem Soc Rev. 2014;43(17):6254-87.

121. Wu Y, Chen F, Huang N, Li J, Wu C, Tan B, et al. Near-infrared light-responsive hybrid hydrogels for the synergistic chemo-photothermal therapy of oral cancer. Nanoscale. 2021;13(40):17168-82.
122. Melo BL, Lima-Sousa R, Alves CG, Moreira AF, Correia IJ, de Melo-Diogo D. Chitosan-based injectable in situ forming hydrogels containing dopamine-reduced graphene oxide and resveratrol for breast cancer chemo-photothermal therapy. Biochemical Engineering Journal. 2022;185:108529.
123. Seo JW, Shin SR, Lee MY, Cha JM, Min KH, Lee SC, et al. Injectable hydrogel derived from chitosan with tunable mechanical properties via hybrid-crosslinking system. Carbohydr Polym. 2021;251:117036.
124. Hamilton M, Harrington S, Dhar P, Stehno-Bittel L. Hyaluronic Acid Hydrogel Microspheres for Slow Release Stem Cell Delivery. ACS Biomaterials Science & Engineering. 2021;7(8):3754-63.
125. Hu M, Yang J, Xu J. Structural and biological investigation of chitosan/hyaluronic acid with silanized-hydroxypropyl methylcellulose as an injectable reinforced interpenetrating network hydrogel for cartilage tissue engineering. Drug Delivery. 2021;28(1):607-19.
126. Deng Y, Ren J, Chen G, Li G, Wu X, Wang G, et al. Injectable in situ cross-linking chitosan-hyaluronic acid based hydrogels for abdominal tissue regeneration. Scientific Reports. 2017;7(1).
127. He J, Chen G, Zhao P, Ou C. Near-infrared light-controllable bufalin delivery from a black phosphorus-hybrid supramolecular hydrogel for synergistic photothermal-chemo tumor therapy. Nano Research. 2021;14(11):3988-98.
128. Zanoni M, Piccinini F, Arienti C, Zamagni A, Santi S, Polico R, et al. 3D tumor spheroid models for in vitro therapeutic screening: a systematic approach to enhance the biological relevance of data obtained. Scientific Reports. 2016;6(1):19103.
129. Gunti S, Hoke ATK, Vu KP, London NR. Organoid and Spheroid Tumor Models: Techniques and Applications. Cancers. 2021;13(4):874.